In vitro reconstitution of an mRNA-transport complex reveals mechanisms of assembly and motor activation

Roland G. Heym,^{1,2,3} Dennis Zimmermann,^{4,6} Franziska T. Edelmann,¹ Lars Israel,⁵ Zeynep Ökten,⁴ David R. Kovar,⁶ and Dierk Niessing^{1,2,3}

¹Institute of Structural Biology, Helmholtz Zentrum München – German Research Center for Environmental Health, 85764 Neuherberg, Germany ²Gene Center, ³Department of Biochemistry, ⁴Institute for Anatomy and Cell Biology, and ⁵Adolf Butenandt Institute, Ludwig-Maximilians University, 81377 Munich, Germany

he assembly and composition of ribonucleic acid (RNA)-transporting particles for asymmetric messenger RNA (mRNA) localization is not well understood. During mitosis of budding yeast, the Swi5p-dependent HO expression (SHE) complex transports a set of mRNAs into the daughter cell. We recombinantly reconstituted the core SHE complex and assessed its properties. The cytoplasmic precomplex contains only one motor and is unable to support continuous transport. However, a defined interaction with a second, RNA-bound precomplex after its nuclear export dimerizes the motor and activates

processive RNA transport. The run length observed in vitro is compatible with long-distance transport in vivo. Surprisingly, SHE complexes that either contain or lack RNA cargo show similar motility properties, demonstrating that the RNA-binding protein and not its cargo activates motility. We further show that SHE complexes have a defined size but multimerize into variable particles upon binding of RNAs with multiple localization elements. Based on these findings, we provide an estimate of number, size, and composition of such multimeric SHE particles in the cell.

Introduction

06 Y

ELL

C

0

mRNA localization by motor-containing transport particles is a widespread mechanism to control gene expression on a spatial and temporal level (Martin and Ephrussi, 2009; Jansen and Niessing, 2012). In higher eukaryotes, such complexes consist of dozens of factors that interact in a largely unknown fashion, resulting in RNA-protein complexes that are actively transported (Marchand et al., 2012). Because of their great complexity, only little information about principles of complex assembly and regulation are available. To date, the most detailed information has been obtained for the yeast *Saccharomyces cerevisiae* (Heym and Niessing, 2012).

R.G. Heym and D. Zimmermann contributed equally to this paper. Correspondence to Dierk Niessing: Niessing@helmholtz-muenchen.de

Z. Ökten's present address is Institute for Molecular and Cellular Biophysics, Technical University Munich, 85748 Munich, Germany.

Abbreviations used in this paper: EDC, 1-ethyl-3-[3-dimethylaminopropyl]-carbodiimide; EMSA, electrophoretic mobility shift assay; NHS, N-hydroxy-succinimide; SEC, size-exclusion chromatography; SHE, Swi5p-dependent HO expression; SLS, static light scattering; TAR, trans-activation response element; TIRF, total internal reflection fluorescence; TIRFM, TIRF microscopy; TMR, tetramethylrhodamine.

During mitotic cell division of S. cerevisiae, ASH1 (asymmetric synthesis of HO 1) mRNA is actively transported to the daughter cell (Long et al., 1997; Takizawa et al., 1997). Localized translation of the protein Ash1p leads to repression of mating type switching exclusively in the daughter cell (Bobola et al., 1996; Sil and Herskowitz, 1996). The Swi5p-dependent HO expression (SHE) complex mediates the active transport of ASH1 mRNA and \sim 30 other transcripts (Takizawa et al., 2000; Shepard et al., 2003; Aronov et al., 2007; Oeffinger et al., 2007; Hogan et al., 2008). In contrast to localizing particles in higher eukaryotes, the core SHE-transport complex consists of only a few components: the RNA-binding proteins She2p and She3p and the type-V myosin Myo4p (Jansen et al., 1996; Böhl et al., 2000; Chung and Takizawa, 2010). Assembly of the SHE complex occurs already cotranscriptionally with the binding of She2p to nascent mRNAs (Shen et al., 2010; Müller et al.,

© 2013 Heym et al. This article is distributed under the terms of an Attribution—Noncommercial—Share Alike—No Mirror Sites license for the first six months after the publication date (see http://www.rupress.org/terms). After six months it is available under a Creative Commons License (Attribution—Noncommercial—Share Alike 3.0 Unported license, as described at http://creativecommons.org/licenses/by-nc-sa/3.0/).

Supplemental Material can be found at: http://jcb.rupress.org/content/suppl/2013/12/20/jcb.201302095.DC1.html

⁶Department of Molecular Genetics and Cell Biology, The University of Chicago, Chicago, IL 60637

2011). After nuclear export, this subcomplex further assembles with She3p and the type-V myosin Myo4p into the mature transport complex (Böhl et al., 2000; Long et al., 2000; Kruse et al., 2002). In this complex, She2p and She3p bind synergistically with high specificity to zip code elements in localizing mRNAs, ensuring the selective transport of target mRNAs (Müller et al., 2011).

Type-V myosins are usually dimeric, which allows for processive movement along actin filaments (Trybus, 2008). In contrast, Myo4p is monomeric and nonprocessive in isolation (Reck-Peterson et al., 2001; Dunn et al., 2007; Heuck et al., 2007; Hodges et al., 2008). Nevertheless, in vivo, the SHE complex supports sustained transport of mRNAs over several micrometers (Bertrand et al., 1998; Beach et al., 1999; Lange et al., 2008).

The crystal structure of She2p revealed a dimeric assembly (Niessing et al., 2004). In solution, two She2p dimers interact to form a tetramer that is required for the recruitment of multiple Myo4p motors (Chung and Takizawa, 2010; Krementsova et al., 2011) and mRNA localization in vivo (Müller et al., 2009). Although one study suggested recruitment of three or more Myo4p motors for processive movement (Dunn et al., 2007; Chung and Takizawa, 2010), a second study reported dimerization of Myo4p in complex with a mutated version of She2p by a mechanism that is not understood to date (Krementsova et al., 2011). It also remains unclear whether the SHE complex forms well-defined or variable molecular arrangements. A major limitation toward such an understanding is that the role of cargo mRNA for mRNP assembly and motor function is not well understood. Furthermore, all previous studies assumed that She3p is a monomer (Dunn et al., 2007; Heuck et al., 2007; Hodges et al., 2008; Bookwalter et al., 2009; Chung and Takizawa, 2010; Heuck et al., 2010; Krementsova et al., 2011), despite the lack of clear experimental evidence.

To date, the most advanced studies on mRNA-transport complexes either work with particles purified from organisms (Chung and Takizawa, 2010; Amrute-Nayak and Bullock, 2012) or involve partial complexes that lack RNA cargo and have been assembled without knowledge of stoichiometric requirements (Krementsova et al., 2011). Studying mRNP assembly of mature RNA-containing complexes under well-defined conditions in vitro would yield stoichiometric ratios and molecular masses of such complexes. It would resolve the question of whether such a complex has a defined molecular mass and, if not, which components control its size. Even more importantly, these insights would explain what effect cargo RNA has on the assembly and activity of a transport complex. To date, these questions remain largely unresolved.

We present a complete stoichiometric in vitro reconstitution of a functional mRNA-transport complex. Determination of size and stoichiometry of the SHE complex revealed that two Myo4p motors associate with one RNA-bound She2p tetramer via two She3p dimers to form a defined complex of almost 1 MD in size. This reconstituted complex processively transports RNA along actin filaments in vitro with a run length that is consistent with long-distance transport in vivo. Whereas the absence of RNA does not greatly alter complex motility, She2p is essential for activation of motility. When investigating the effect of cargo

RNA with multiple zip code elements, we observed clustering of SHE complexes into large assemblies. These multimeric particles show motilities very similar to single zip code RNA–containing particles. By combining known cellular copy numbers of SHE factors and our results on complex assembly, we provide an estimate on the number, molecular mass, and composition of SHE particles in the cell.

Results

She3p oligomerizes via its N terminus

Previous studies showed that isolated Myo4p is a monomer (Dunn et al., 2007; Heuck et al., 2007; Hodges et al., 2008) and She2p is a tetramer in solution (Müller et al., 2009; Chung and Takizawa, 2010). The oligomeric state of She3p has not been addressed so far. We used bacterially expressed N- and C-terminal fragments of She3p and baculovirus-expressed full-length She3p to investigate its oligomeric state by chemical crosslinking with 1-ethyl-3-[3-dimethylaminopropyl]carbodiimide (EDC) and N-hydroxysuccinimide (NHS; Fig. S1, A and B). This experiment revealed oligomerization of She3p via its N-terminal half (amino acids 1–234; Fig. S1 B). In contrast, the C terminus of She3p (amino acids 274–425) was not crosslinked. Also, the C terminus of bacterially expressed monomeric Myo4p (Myo4p-C) failed to show cross-linking (Fig. S1 A). Although the exact determination of oligomeric states by crosslinking has to be considered with caution, the migration of the main cross-linking product of She3p in SDS-PAGE suggests the formation of a She3p dimer.

One She3p dimer and one Myo4p monomer form a stable complex

For efficient cargo transport, the monomeric Myo4p requires oligomerization (Chung and Takizawa, 2010; Krementsova et al., 2011). In the cytoplasm, Myo4p forms a stable, high affinity complex with She3p (Heuck et al., 2007; Hodges et al., 2008). Hence, a She3p dimer might provide a way to promote such an oligomerization of Myo4p.

To test this possibility, we determined the stoichiometry and the molecular mass of the She3p:Myo4p-C complex. Isothermal titration calorimetry experiments indicated a stoichiometric ratio of two She3p molecules to one Myo4p-C molecule (Fig. 1 A). A titration by size-exclusion chromatography (SEC) confirmed this result (Fig. S1 C). Quantitative mass spectrometry with heavy isotope-labeled peptides yielded a stoichiometric ratio of 2.56 ± 0.11 for She3p:Myo4p-C (Fig. 1 B). These experiments indicate a stoichiometric ratio of 2:1 for the She3p: Myo4p-C complex and suggest a She3p dimer or multimers thereof in the co-complex.

In line with previous studies (Dunn et al., 2007; Heuck et al., 2007; Hodges et al., 2008), molecular mass determination by static light scattering (SLS) confirmed that recombinant Myo4p-C is a monomer (Fig. 1 C and Table 1). SLS with the complex of She3p and Myo4p-C yielded a molecular mass of $160.2 \pm 3.6 \, \text{kD}$ (Fig. 1 D and Table 1) and suggests a complex of one She3p dimer and one Myo4p monomer. Thus, oligomerization of Myo4p does not occur at this step of assembly.

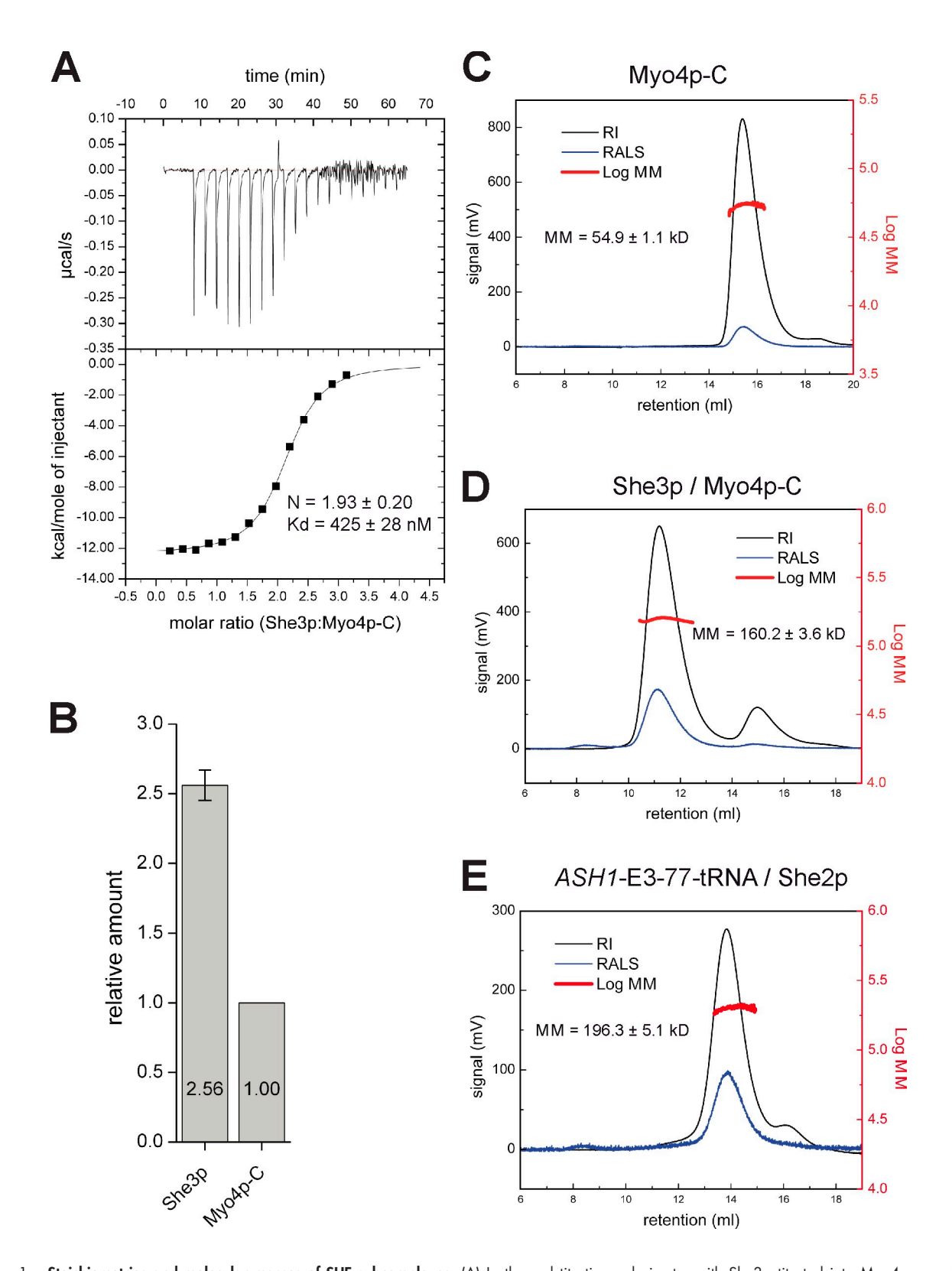


Figure 1. Stoichiometries and molecular masses of SHE subcomplexes. (A) Isothermal titration calorimetry with She3p titrated into Myo4p revealed a stoichiometry of 1.93 ± 0.20 (mean and standard deviation of two experiments) for the She3p:Myo4p complex. (B) Quantitative mass spectrometry with heavy isotope-labeled peptides showed a stoichiometry of 2.56 ± 0.11 (mean and standard deviation of two independent experiments) for the She3p: Myo4p complex. The amount of She3p was normalized with respect to Myo4p. (C) SLS profile of Myo4p shows that this protein is monomeric. RI, refractive index; RALS, right angle light scattering; MM, fitted molecular mass. (D) SLS profile of the She3p:Myo4p complex. Note that a slight excess of Myo4p was used to ensure saturation of the complex. (E) SLS profile of the ASH1-E3-77-tRNA:She2p complex.

Table 1. Analysis of complex assemblies by SLS

Sample	MM exp.	MM calc.	Copy no.
	kD	kD	
Муо4р-С	54.9 ± 1.1	56.7	1
She3p/Myo4p-C	160.2 ± 3.6	153.2	2/1
ASH1-E3-51/She2p	139.2 ± 8.0	147.2	2/4
ASH1-E3-77-tRNA/She2p	196.3 ± 5.1	211.8	2/4
IST2-tRNA/She2p	176.6 ± 2.6	202.1	2/4
ASH1-E3-77-tRNA/She2p/ She3p/Myo4p-C	502.8 ± 9.8	518.2	2/4/4/2

Molecular masses from experimental SLS analysis (MM exp.) compared with calculated molecular masses (MM calc.) for complexes with the indicated copy number of proteins and RNAs. Data represent the means and standard deviation of at least three experiments with varying sample concentrations. Calculated theoretical molecular masses of the monomers are as follows: 56.7 kD (Myo4-C), 48.2 kD (She3p), 28.7 kD (She2p), 16.3 kD (ASH1-E3-51), 48.7 kD (ASH1-E3-77:HRNA), and 43.7 kD (IST2-HRNA).

One She2p tetramer binds two zip code RNAs

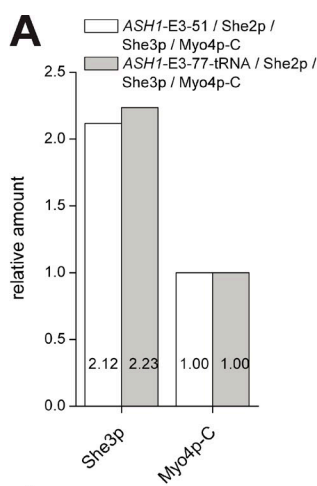
In the nucleus, She2p preassembles with *ASH1* mRNA (Kruse et al., 2002; Shen et al., 2010; Müller et al., 2011). Efficient mRNA binding and localization require the formation of She2p tetramers (Müller et al., 2009; Chung and Takizawa, 2010).

As different stoichiometric ratios have been suggested for She2p RNA complexes (Niessing et al., 2004; Olivier et al., 2005), we determined the molecular mass of bacterially expressed She2p in complex with a 77-nucleotide ASH1-E3 zip code RNA fused to tRNA (ASH1-E3-77-tRNA) by SLS. The tRNA tag was used to produce large amounts of stable RNA (Ponchon and Dardel, 2007). The measured molecular mass suggests that one She2p tetramer binds two ASH1-E3 RNAs (Fig. 1 E and Table 1), which is in agreement with a previous study (Niessing et al., 2004). We also observed complex formation between two zip code elements and one She2p tetramer with a 51-nucleotide-long ASH1-E3 RNA lacking the tRNA tag (Fig. S1 D) and with the IST2 zip code RNA fused to tRNA (Fig. S1 E). In summary, the data indicate that the ASH1-E3 and the IST2 zip code elements bind the She2p tetramer with the same stoichiometry.

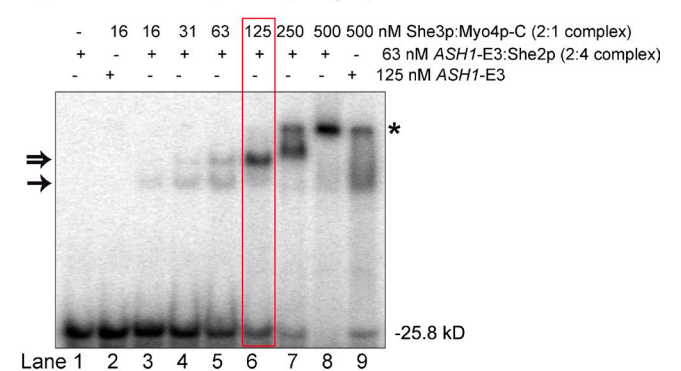
Assembly of the SHE core complex induces Myo4p dimerization

When the RNA:She2p subcomplex reaches the cytoplasm, it associates with the single-headed subcomplex of She3p and Myo4p. We reasoned that Myo4p oligomerization is likely to occur during this final step of assembly. To determine the protein stoichiometries in the SHE core complex, we performed quantitative mass spectrometry with heavy isotope-labeled peptides. The stoichiometric ratio between She3p and Myo4p-C was 2.12 in a SHE core complex reconstituted with *ASH1*-E3-51 RNA and 2.23 in a SHE core complex reconstituted with *ASH1*-E3-77-tRNA (Fig. 2 A). Thus, the stoichiometry between She3p and Myo4p in the SHE core complex is the same as in the She3p:Myo4p-C subcomplex (compare with Fig. 1, A and B).

We performed electrophoretic mobility shift assays (EMSAs) to investigate the stoichiometry of the assembly between the RNA:She2p and the She3p:Myo4p-C subcomplex







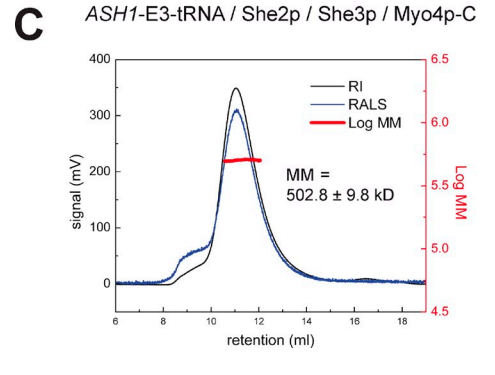


Figure 2. Assembly of the SHE core complex induces Myo4p dimerization. (A) Quantitative mass spectrometry of the SHE core complex reconstituted with ASH1-E3-51 or ASH1-E3-77-tRNA. Heavy isotope-labeled peptides of She3p and Myo4p-C were used for quantification. The stoichiometry of the She3p:Myo4p-C interaction was 2.12 (ASH1-E3-51 complex) or 2.23 (ASH1-E3-77-tRNA complex). (B) The stoichiometry of the SHE core complex was determined by EMSA with radioactively labeled RNA. A constant concentration of ASH1-E3-77:She2p (2:4) subcomplex was used, and increasing concentrations of She3p:Myo4p-C (2:1) subcomplex were titrated. The distinct band observed in lane 6 (double arrow and red box) indicates binding of two She3p:Myo4p subcomplexes to one RNAbound She2p tetramer. The single arrow marks a substoichiometric SHE core complex, and the asterisk marks a high molecular mass complex between the RNA in the SHE core complex and excess She3p:Myo4p-C with unspecific RNA-binding properties. (C) SLS profile of the SHE core complex containing ASH1-E3-77-tRNA, She2p, She3p, and Myo4p-C. RI, refractive index; RALS, right angle light scattering; MM, fitted molecular mass.

(Fig. 2 B). A constant amount of 63-nM unlabeled *ASH1*-E3-77: She2p (2:4) subcomplex was titrated with increasing amounts of the She3p:Myo4p-C (2:1) subcomplex. In a control experiment,

She2p on its own was unable to induce a mobility shift (Fig. 2 B, lane 1), whereas high concentrations of She3p:Myo4p-C in the absence of She2p resulted in a strong shift to high-molecular mass complexes (Fig. 2 B, lane 9, asterisk). We observed similar unspecific RNA binding of She3p in the absence of She2p in a previous study (Müller et al., 2011). At a ratio of two She3p: Myo4p-C subcomplexes to one RNA-bound She2p tetramer, a single band appeared (Fig. 2 B, lane 6, double arrow), indicating the formation of a homogeneous, stoichiometric complex. At a lower titration concentration, at which ASH1-E3-77:She2p was not yet saturated with She3p:Myo4p-C, an additional band emerged, indicating formation of a smaller complex (Fig. 2 B, lanes 3–5, single arrow). It is likely that this complex consists of a She2p tetramer that is bound by only one She3p:Myo4p-C subcomplex, leaving one binding site of She2p free. In contrast, when She3p:Myo4p-C was added in excess, a higher molecular mass band appeared at the size of the unspecific RNA binding observed with She3p:Myo4p alone (Fig. 2 B, lanes 7–9, asterisk). Control EMSAs suggest that this increase in size is not simply caused by concentration-dependent aggregation but rather reflects unspecific binding of excess She3p:Myo4p subcomplexes to the RNA in the SHE core complex (Fig. S2). In summary, the EMSA analyses suggest that two She3p:Myo4p-C subcomplexes associate with one RNA-bound She2p tetramer to form a SHE core complex with defined size. This complex between ASH1-E3-77, She2p, She3p, and Myo4p has a stoichiometric ratio of 1:2:2:1 and most likely consists of two ASH1-E3-77 RNAs, a She2p tetramer, two She3p dimers, and two Myo4p monomers.

To validate the EMSA titration, we performed SEC experiments. In the first experiment, equimolar amounts of She2p and She3p were incubated with concentrations of *ASH1*-E3-51 RNA and Myo4p slightly exceeding the determined stoichiometric ratio. This resulted in a homogeneous complex of all the components but without excess of *ASH1*-E3:She2p (Fig. S3 A). In contrast, if a twofold molar excess of She2p over She3p was used, a large amount of *ASH1*-E3:She2p was separated from the quaternary SHE core complex (Fig. S3 B). In agreement with the EMSA analysis, these experiments indicate that the SHE core complex is saturated at equimolar amounts of She2p and She3p.

To determine the copy numbers of its components, we measured the molecular mass of the SHE core complex by SLS. We used again the tRNA-tagged ASH1-E3-77 RNA for reconstitution. For a SHE core complex consisting of ASH1-E3-77-tRNA, She2p, She3p, and Myo4p-C, a molecular mass of 502.8 ± 9.8 kD was measured (Fig. 2 C and Table 1). This result is consistent with our stoichiometry determination and suggests binding of two She3p:Myo4p-C subcomplexes to one RNA-bound She2p tetramer.

In summary, stoichiometry and molecular mass analyses indicate that the She2p tetramer provides a platform for binding of two zip code RNAs and two She3p:Myo4p-C subcomplexes. These components assemble into a defined SHE core complex of $\sim\!500$ kD. Considering full-length Myo4p bound by six light chains, a single SHE complex has a molecular mass of 835 kD plus its bound mRNA.

RNAs with two zip code elements induce clustering of SHE core complexes

So far, we characterized the assembly of SHE core complexes with RNAs containing single zip code elements. However, transported mRNAs, such as *ASH1*, *WSC2*, or *DNM1* mRNA, contain more than one zip code element (Chartrand et al., 1999; Gonzalez et al., 1999; Jambhekar et al., 2005). Because She2p has two binding sites for zip code elements, multi–zip code RNAs and SHE complexes could potentially multimerize into large particles of variable size.

To test this possibility, we designed an RNA construct, in which two ASH1-E3 elements were fused to the tRNA tag via a three-way junction from the Twort intron (Fig. 3 B; Lescoute and Westhof, 2006). This RNA was reconstituted with SHE core complexes and analyzed by dynamic light scattering and sucrose density gradient centrifugation. Compared with a SHE core complex with a single ASH1-E3 zip code (Fig. 3 A), this complex showed a marked increase in the hydrodynamic radius as well as faster sedimentation (Fig. 3 B). When assuming an idealized globular particle shape, this increase in hydrodynamic radius translates into an >100-fold increase of its volume, indicating that a large number of SHE core complexes are cross-linked into one particle. The broad distribution of these complexes in the sucrose gradient (Fig. 3 B, fractions 2-5) further indicates that a range of multimers with variable particle sizes was formed. This behavior is well explained by the association of two bivalent interaction partners. As a control, a tRNA fused to a three-way junction with one ASH1-E3 zip code and one HIV-1 trans-activation response element (TAR) stem loop was used (Fig. 3 C). This RNA behaved similar to ASH1-E3-tRNA (Fig. 3 A). The HIV-1 TAR stem loop fused to tRNA also failed to induce complex formation (Fig. 3 D). In summary, these experiments demonstrate that an RNA containing at least two zip code elements is able to multimerize SHE core complexes. This might provide a way to incorporate several mRNAs and multiple motors into one particle.

Reconstituted SHE complexes move processively along actin in vitro

The incorporation of two Myo4p motors suggests that reconstituted SHE complexes indeed move processively along actin filaments. To test this assumption, we performed in vitro single-particle motility assays. We copurified full-length, FLAG-tagged Myo4p with She3p, She4p, calmodulin (Cmd1p), and myosin light chain (Mlc1p) after baculovirus expression and used this preparation for reconstitution with bacterially expressed GFP-She2p. As cargo RNA, we used a fragment of the *ASH1* mRNA containing one E3 zip code element (*ASH1-3'*; Table S5). Particles were visualized via GFP and total internal reflection fluorescence (TIRF) microscopy (TIRFM).

ASH1-3' RNA—containing particles were transported with a mean velocity of 0.74 ± 0.20 µm/s (mean and standard deviation) and run length of 2.13 ± 0.89 µm along actin filaments (Fig. 4, A, E, and F; and Video 1). The observed velocity is only moderately higher than published velocities of SHE particles in yeast cells (200–440 nm/s [Bertrand et al., 1998], 546 nm/s [Lange et al., 2008], and 630 nm/s [Beach et al., 1999]). Thus,

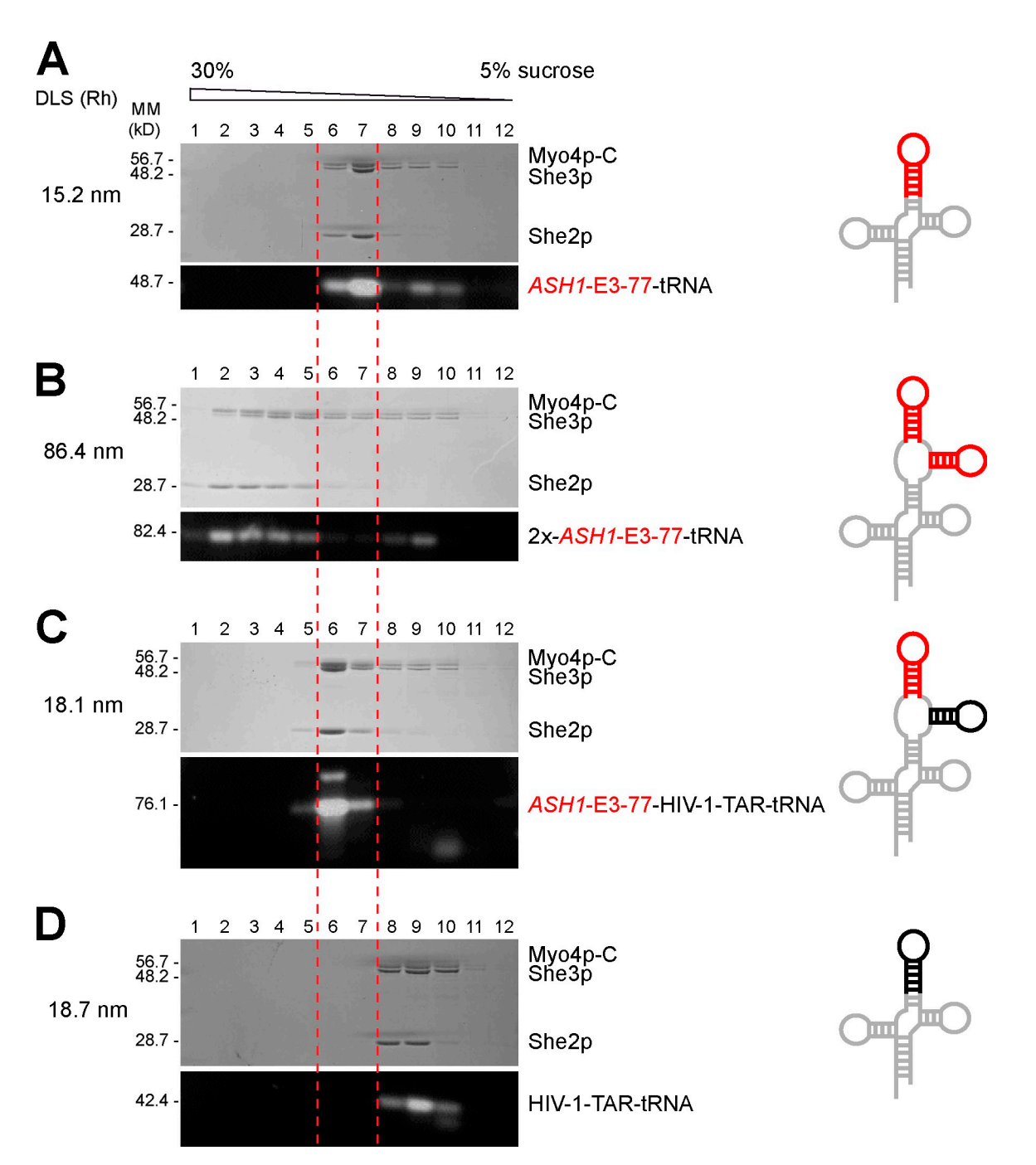


Figure 3. An RNA with two zip code elements induces multimerization of SHE core complexes. (A–D) Dynamic light scattering (DLS) analysis and sucrose density gradient centrifugation of SHE core complexes with different RNA constructs. An RNA containing two zip code elements (B) induced the formation of much bigger complexes than RNA with only one zip code element (A and C). The increased hydrodynamic radius (Rh; numbers given in nanometer) and the faster sedimentation indicate multimerization of SHE core complexes in the presence of 2× ASH1-E3-774RNA. Furthermore, the broad distribution of complexes in the gradient suggests that a range of complex sizes was formed. No stable RNA complexe formation was detected with HIV-1 TAR4RNA (D), and only smaller subcomplexes co-migrated in the sucrose gradient. Fractions were analyzed by SDS-PAGE (proteins) with Coomassie blue staining and agarose gel electrophoresis (RNA) with GelRed staining. Schematics of the RNA constructs are shown on the right. Distinct features are color coded: ASH1-E3-77 (red), HIV-1 TAR (black), and three-way junction and tRNA (gray). Red dotted lines mark fractions 6 and 7, which contained the co-complex with a single zip code element (A).

our data are in good agreement with in vivo events. For a subset of these motile particles, photobleaching experiments were performed. As an internal control, we also assessed the bleaching step profiles of She2-GFP protein alone. The results indicate that motile particles with a single zip code element indeed contain only up to four GFP fluorophores and thus a single SHE complex (Fig. S4, A—C).

RNA cargo is dispensable for processive particle transport

To test the requirement of RNA cargo for processive movement, particles lacking RNA were targeted for TIRFM motility assays by visualizing GFP-labeled She2p. The mean velocity centered around $0.65 \pm 0.15 \,\mu\text{m/s}$, whereas the determined mean run length was $2.48 \pm 1.02 \,\mu\text{m}$ (Fig. 4, B, E,

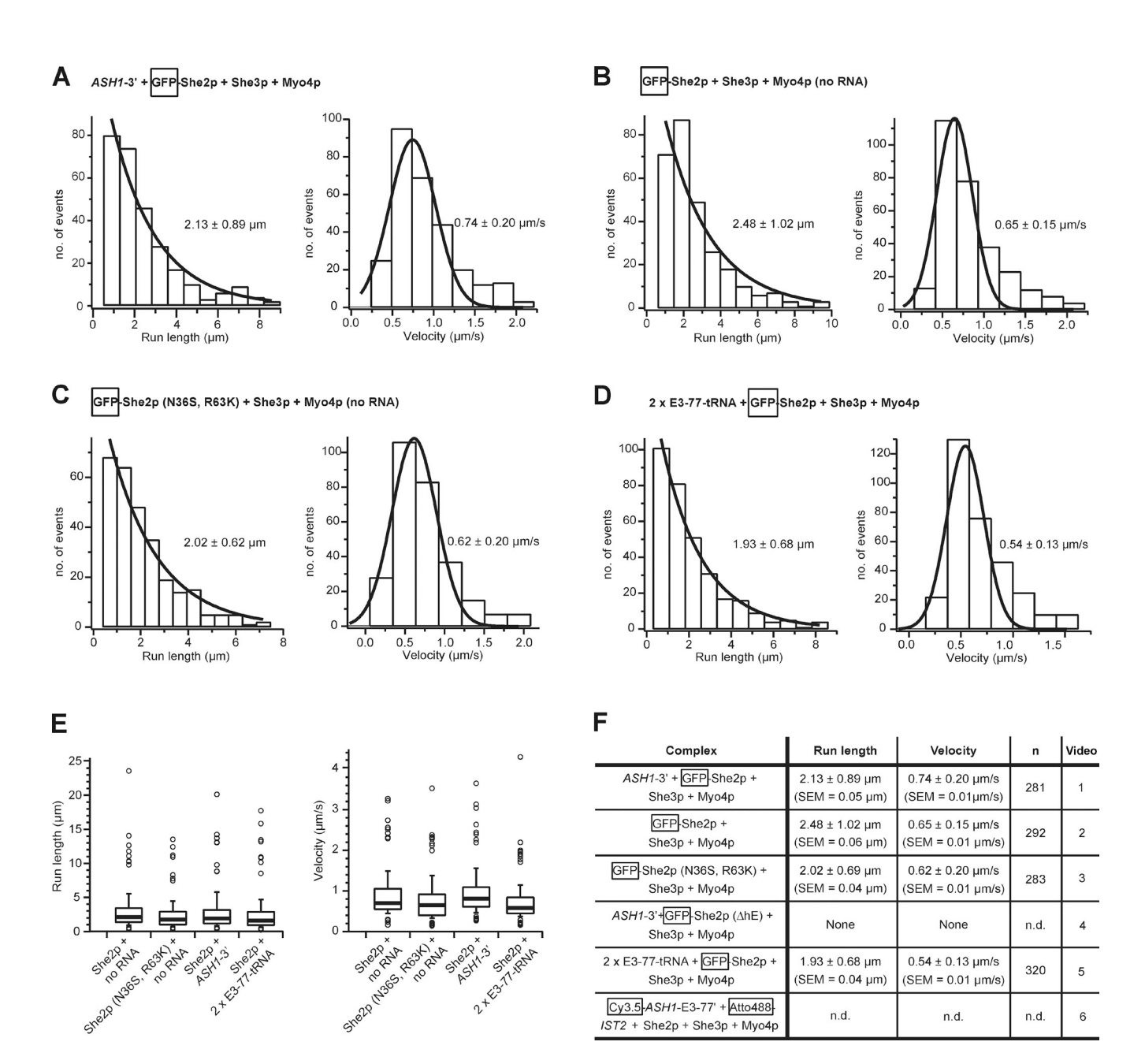


Figure 4. **Single-particle motility assays with different SHE complexes visualized by TIRFM.** (A) Single-particle motility of SHE complexes in the presence of *ASH1-3*′ RNA containing one E3 zip code element. 281 processive runs were analyzed. (B) Single-particle motility assay of the SHE complex in the absence of zip code RNA. 292 processive runs were analyzed. The presence of zip code RNA does not greatly change the motility properties of the SHE complex. (C) Single-particle motility assay of SHE complex with the RNA binding-deficient She2p (N365, R63K) mutant confirms that the RNA cargo is dispensable for processive movement. 283 processive runs were analyzed. (D) Single-particle motility assays with RNA containing two zip code elements fail to show enhanced processivity. Mean run length and velocity of a tRNA fusion construct with two *ASH1*-E3 zip code elements are even slightly reduced compared with particles with only a single zip code RNA. (E) Box plots representing data distributions for run lengths and velocities of each experiment, except for *ASH1-3*′ and *IST2* RNA together. Here, the number of particles is too low for valid statistical analyses. Outliers (open circles, for details see Materials and methods) were determined to confirm the homogeneity in the collected data. Only a small number (*n* < 28) represent outliers; thus, all the events herein analyzed were considered representative for the respective experimental condition. The bold black lines show the median, the boxed regions indicate the first and third quartiles, and the whiskers above and below show the limits for outliers. (F) Table summarizing results from the different single-particle motility assays. The mean values for run length (left) and velocity (right) are derived from single-exponential and Gaussian fits to the distributions, respectively. All data derive from TIRFM motility assays, in which the GFP from the GFP-She2p fusion protein was visualized (as indicated by the boxed molecule name in the complex descriptions), unless

and F; and Video 2). A comparison of these values with motilities in presence of RNA (Fig. 4, A and F) suggests that RNA cargo does not activate processivity.

A potential limitation of this interpretation is that residual RNA contaminations from the insect cell purification might still

be present in the supposedly RNA-free protein preparations. Thus, such RNA contaminations could bind to the She2p:She3p complex and potentially promote motility. To exclude this possibility, we performed TIRFM motility assays with particles containing the GFP-She2p mutant (N36S, R63K), which is defective

in binding to RNA (Du et al., 2008). Corresponding SHE complexes moved with a mean velocity of $0.62 \pm 0.20 \,\mu\text{m/s}$ and run length of $2.02 \pm 0.69 \,\mu m$ along actin filaments (Fig. 4, C, E, and F; and Video 3). As these values are comparable to wild-type particles, it confirms that RNA per se is dispensable for the processive movement of SHE complexes.

She2p:She3p interaction is essential for motility

A She2p mutant lacking its protruding helix E (She2p $[\Delta hE]$) fails to interact with She3p (Müller et al., 2011). If the interaction between She2p and She3p rather than the cargo RNA is essential for motility, SHE particles containing the She2p (ΔhE) mutant should not move processively along actin filaments. To test this, we reconstituted GFP-She2p (ΔhE)-containing particles and traced their motility via GFP and TIRFM. Indeed, for these complexes, no motility on F-actin was observed under otherwise identical experimental conditions (Fig. 4 F and Video 4). This experiment confirms that the interaction between She2p and She3p is essential for SHE complex motility.

SHE complexes with a two zip code RNA show no increased processivity

ASH1 mRNA has four zip code elements. In vitro, already, two zip code elements multimerize SHE complexes into large particles (Fig. 3). To find out what effect multiple zip codes per RNA have on particle movement, we performed TIRFM motility assays with the 2× ASH1-E3-77-tRNA construct (Fig. 3 B) and GFP-She2p-containing particles. 2× ASH1-E3-77-tRNA particles were on average brighter than observed with a single zip code RNA (Video 5; compare with Video 1). As expected, the here-performed photobleaching experiments show that particles containing 2× ASH1-E3-77-tRNA show twice as many fluorescence intensity populations than particles with ASH1-3' (Fig. S4, D and E). Along those lines, in photobleaching experiments, over 65% of the 2x ASH1-E3-77-tRNA particles analyzed showed more steps in photobleaching than the majority of particles with a single zip code RNA (30 processive runs were analyzed). The mean velocity of particles with $2 \times ASH1$ -E3-77tRNA was $0.54 \pm 0.13 \,\mu\text{m/s}$, and the run length was $1.93 \pm$ 0.68 µm (Fig. 4, D-F). These motility parameters are in close range of particles bound to RNA with a single zip code element (Fig. 4 F). In summary, these data suggest that particles with 2× ASH1-E3-77-tRNA contain oligomerized SHE complexes and that these multimeric particles move with velocities and mean run lengths that are indistinguishable from particles with a single SHE complex.

SHE complexes can simultaneously transport two RNA species

In vivo transport of ASH1 and IST2 mRNA to the bud tip is sometimes accomplished by the same particle (Lange et al., 2008). To find out whether our reconstituted particles can recapitulate this feature, we fluorescently labeled ASH1-E3-77 and the IST2 zip code element with Cy3.5 and Atto488 fluorophores, respectively. Motility assays revealed that some of the motile particles indeed contained both fluorophores (Fig. 4 F and Video 6), indicating that two different RNAs can be transported by the same reconstituted SHE complex particle. Because fluorophores were directly attached to the RNA, this experiment also serves as direct proof that the reconstituted particles indeed transport RNA cargo.

Discussion

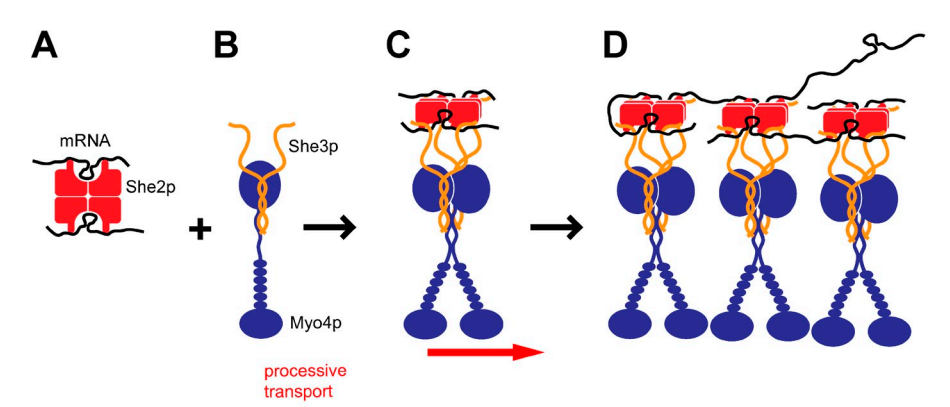
Here, we fully reconstituted a functional mRNA-transport complex including all recombinantly expressed core proteins together with RNA in their correct stoichiometries. We show that the individual components assemble with fixed copy numbers to form a defined complex with a molecular mass of \sim 835 kD plus bound mRNA. This complex processively transports RNA containing a single zip code element with physiological run length and velocity in vitro. We further show that in the presence of RNAs with more than one zip code element, several SHE complexes undergo higher-order assembly into large, polydisperse particles. This finding resolves several previously contradictory findings on Myo4p multimerization (Dunn et al., 2007; Heuck et al., 2007; Bookwalter et al., 2009; Chung and Takizawa, 2010; Krementsova et al., 2011).

Previous assessments of She3p:Myo4p complexes assumed a monomeric She3p (Dunn et al., 2007; Hodges et al., 2008). Our chemical cross-linking experiments suggest that She3p dimerizes via its N terminus, where a predicted coiledcoil region of >100 amino acids could potentially mediate dimerization. In this respect, She3p is reminiscent of organelle adapter proteins of type-V myosins, which often contain coiled coils and dimerize (Li and Nebenführ, 2008).

Myo4p forms a constitutive complex with She3p (Dunn et al., 2007; Heuck et al., 2007; Hodges et al., 2008). One study suggested that this subcomplex contains only one myosin (Hodges et al., 2008), whereas another study showed that artificial dimerization of Myo4p stabilizes its interaction with She3p, suggesting dimerization of Myo4p in this subcomplex (Heuck et al., 2007). In a third study, chemical cross-linking suggested a complex of one Myo4p and one She3p (Dunn et al., 2007). Here, we used quantitative interaction studies to show that one She3p dimer binds to one Myo4p monomer, forming a singleheaded motor complex (Fig. 5 B). This finding suggests that the She3p:Myo4p subcomplex alone is unable to support processive movement. Indeed, we found that SHE complexes with the She2p (ΔhE) mutant, in which She2p and the She3p:Myo4p subcomplex fail to interact, do not show any processive movement (Video 4).

She2p assembles into a tetramer with two large, continuous RNA-binding surfaces on opposite sides (Müller et al., 2009). Because different stoichiometric ratios for RNA:She2p complexes have been suggested for different zip code elements (Niessing et al., 2004; Olivier et al., 2005), we measured the molecular mass of She2p in complex with ASH1-E3 zip code RNA. Our results suggest binding of two zip code elements to one She2p tetramer (Fig. 5 A), which is consistent with the stoichiometry suggested by us in an earlier study (Niessing et al., 2004).

When the subcomplex of ASH1 mRNA and She2p reaches the cytoplasm, it interacts with the preassembled She3p:Myo4p Ε



■)S		ASH1 mRNAs	mRNAs	SHE complexes	MM of particle	Particles
		per particle *	per particle	per particle	20	per cell
	Min	2.4	3.9	6.9	8.0 MD	36.7
	Average	7.2	11.6	20.6	24.1 MD	12.2
	Max.	15.6	25.2	44.7	52.3 MD	5.6

of SHE complexes. Because the She2p tetramer has two RNA binding sites, several RNAs are incorporated, and large mRNPs of variable size are formed. Such higher-order mRNPs contain multiple Myo4p dimers that might enhance sustained transport in vivo (Chartrand et al., 2002; Chung and Takizawa, 2010). (E) Calculation of SHE particle properties in cells based on our model, the minimal/mean/maximal number of ASH1 mRNAs observed per transport particle in vivo (marked by an asterisk; Haim et al., 2007), and the reported 88 ASH1 mRNA copies per cell (Trcek et al., 2012). Details on the calculation are given in the Materials and methods section and in Tables S1 and S2.

subcomplex to form the mature transport complex (Kruse et al., 2002; Müller et al., 2011). Our analyses of the size and stoichiometry suggest that one RNA-bound She2p tetramer recruits two She3p:Myo4p subcomplexes (Fig. 5 C). Thus, the She2p tetramer provides a scaffold for dimerization of Myo4p. This result is consistent with the previous finding that a single transport complex purified from yeast cells contains at least two Myo4p molecules (Chung and Takizawa, 2010).

Another previous study showed that active mRNA transport is achieved in Δ*SHE*2 cells, when She3p is fused to an MS2 coat protein and *ASH1* mRNA is fused to MS2-target stem loops in its 3'UTR (Kruse et al., 2002). The authors concluded that the only function of She2p might be the tethering of *ASH1* mRNA to the motor complex. However, the work presented here as well as previous studies (Müller et al., 2011; Sladewski et al., 2013) indicates that She2p plays a more central role. The mechanistic requirement of defined stoichiometries provided here (Fig. 5, A–D) suggests a potential rationale for the observation by Kruse et al. (2002). Because MS2 coat proteins form dimers, it is likely that individual Myo4p:She3p-MS2 complexes are dimerized by the MS2 coat protein. As a result, processive movement could potentially be activated in a manner, which is reminiscent of the activation by She2p.

Our in vitro reconstitution experiments suggested equimolar concentrations of myosin and RNA in the SHE particles. Thus, we also performed single particle motility assays with equimolar concentrations of myosin and RNA (Fig. 4). The observed mean run length of particles with single zip code RNAs was 2.13 μm , which is significantly higher than observed in a concurrent study (0.9–1.4 μm ; Sladewski et al., 2013). In summary, our observation suggests that in vivo, some SHE particles are likely capable of moving the entire distance to the bud tip ($\sim\!2$ –4 μm , depending on the size of the bud cell; Lange et al., 2008) with one continuous run.

Figure 5. Model of stepwise SHE complex assembly. (A) One She2p tetramer (red) binds two zip code RNAs (black). In the presence of transcripts with two or more zip code elements, higher-order assembly (as shown in D) might occur already at this stage. (B) One Myo4p monomer (blue) forms a constitutive co-complex with one She3p dimer (orange). The N-terminal coiled-coil mediates dimerization of She3p as well as interaction with the Myo4p C terminus. This single-headed motor complex is unable to promote processive transport (Dunn et al., 2007; Hodges et al., 2008). (C) The RNA:She2p subcomplex assembles with two Myo4p:She3p subcomplexes forming the mature SHE complex. The C terminus of She3p binds directly to zip code RNA and to helix E of She2p (Müller et al., 2011). This interaction ensures highly specific RNA recognition and incorporates two Myo4p copies into one mRNP. She2p-mediated dimerization of Myo4p enables processive transport of the SHE complex. (D) Transcripts with more than one zip code element induce multimerization

ASH1-3' RNA-containing particles had a mean velocity of 0.74 µm/s in TIRFM experiments, which is also in good agreement with previous actin gliding assays (0.45–0.65 μm/s; Dunn et al., 2007) and in vivo observations of localizing particles (0.55 µm/s [Lange et al., 2008], 0.20–0.44 µm/s [Bertrand et al., 1998], and 0.63 µm/s [Beach et al., 1999]). To date, the effect of RNA cargo binding on particle motility remains unclear. To elucidate this issue, we used particles that were either assembled in the absence of RNA or assembled with the RNA binding-deficient She2p (N36S, R63K) mutant. Both types of experiments yielded similar run lengths (2.48 and 2.02 µm, respectively) and slightly decreased velocities (0.65 and 0.62 µm/s, respectively) when compared with ASH1-3'-loaded particles (run length: 2.13 μm; velocity: 0.74 μm/s). Also, a comparison of the motile events per F-actin length and acquisition time for the different reconstituted SHE complexes did not show any positive effect of RNA binding on the interaction and subsequent transport of those SHE particles on F-actin (Fig. S5). In summary, we conclude that the rather small differences in run length with or without RNA are not pointing toward an RNAdependent activation of processive movement.

ASH1 mRNA and a subset of other localizing RNAs contain more than one zip code element (Takizawa et al., 2000; Shepard et al., 2003; Aronov et al., 2007; Oeffinger et al., 2007; Hogan et al., 2008). Our in vitro experiments showed that an RNA consisting of a tRNA fused to two ASH1-E3 elements cross-links SHE complexes into large particles (Fig. 3). To further test the potential effect of such multimerization events, we performed single particle motility assays with a SHE complex containing such a double zip code RNA. In TIRFM experiments, the mean run length of these particles (1.93 μm) was essentially unchanged from the run length of the single zip code ASH1-3′ RNA (2.13 μm). Also, their mean velocity of 0.54 μm/s provides evidence against an RNA-based activation mechanism (velocity

of ASH1-3' particle: 0.74 μ m/s) as did the analysis of numbers of motile particles per micrometer actin filament and time (Fig. S5). However, the measured values with the double zip code RNA are again in good agreement with in vivo observations of localizing particles (0.55 μ m/s [Lange et al., 2008], 0.20–0.44 μ m/s [Bertrand et al., 1998], and 0.63 μ m [Beach et al., 1999]).

Concurrent to our study, Sladewski et al. (2013) showed that the mean run lengths of SHE particles become longer with increasing numbers of zip code elements per RNA (multi–zip code RNAs: 1.1–1.5 µm; single zip code RNAs: 0.9–1.3 µm). These experiments were performed at a strong substoichiometric ratio of RNA over myosin (0.035 nM RNA and 25 nM myosin). At much higher concentrations of myosin (250 nM) and RNA (10 nM), run lengths with an eight–zip code element RNA increased to 2.8 µm (1.4 µm for a single zip code; Sladewski et al., 2013). Bleaching and electron microscopy images suggested that a strong underrepresentation of RNA results in particles in which a single multi–zip code RNA is bound to up to four motor complexes and little cross-linking into large particles occurs (Sladewski et al., 2013).

Guided by our in vitro reconstitution study, we performed TIRFM experiments at equimolar conditions of RNA and Myo4p. A calculation of particle numbers per cell also suggests near-stoichiometric conditions in the cell (see following paragraphs of the Discussion; Fig. 5 E and Tables S1 and S2). We found that particles with single zip code elements or even without RNA are already sufficient for processive movement over distances that are close to the ones from the perinuclear regions to the bud tips of dividing yeast cells (Fig. 4). It might well be that the different stoichiometries in SHE complexes of both experiments are responsible for the different observations. In summary, increased run lengths by multi–zip code RNA might be a relevant mechanism in vivo that is perhaps not essential for RNA localization in the cell.

Additional experimental differences between both observations exist as well. We used wild-type She2p and skeletal muscle actin from rabbits. In the concurrent publication, experiments were performed with She2p bearing four point mutations (all cysteines to serines) and yeast actin that had been tropomyosin stabilized (Sladewski et al., 2013). The mutant version of She2p was reported to rescue *ASH1* mRNA localization in vivo and thus seems to be at least partially functional (Krementsova et al., 2011). In our hands, thoroughly purified wild-type She2p (see Materials and methods) is monodisperse and well behaved (Müller et al., 2009, 2011). Therefore, we performed all our experiments with wild-type She2p.

In vivo particle-tracking experiments with two differently labeled RNA species showed that different RNA species can be transported in one particle (Lange et al., 2008). By using in vitro–reconstituted SHE particles containing *ASH1*-E3 and *IST2* RNAs that were labeled with Cy3.5 and Atto488 fluorophores, respectively, we recapitulated this observation in vitro. It also supports our in vitro observation that an individual SHE complex is able to bind two independent RNA molecules.

Several localizing transcripts, such as *ASH1*, *WSC2*, and *DNM1* mRNA, contain two or more zip code elements (Chartrand

et al., 1999; Gonzalez et al., 1999; Jambhekar et al., 2005), suggesting multimerization of transport complexes by different RNAs (Fig. 5 D). The observed multimerization by multi–zip code RNAs explains why overexpression of *ASH1* mRNA leads to fewer, but larger, particles in the cell (Bertrand et al., 1998; Lange et al., 2008).

Interestingly, higher-order assemblies have also been described for *oskar* mRNA-transport complexes in *Drosophila melanogaster* oocytes (Besse et al., 2009). The formation of these large *oskar* mRNPs is thought to serve two functions: first, the efficient co-transport of several transcripts and second, their translational repression during transport. In analogy, the formation of large SHE particles through RNA-mediated multimerization could serve very similar purposes.

Previous studies determined the number of ASH1 mRNAs present in a single transport particle in vivo as well as the number of ASH1 mRNAs in a dividing yeast cell (Haim et al., 2007; Trcek et al., 2012). Using this information, we calculated that between 6 and 37 SHE particles are present in one cell (Fig. 5 E). This is consistent with the number of particles observed by fluorescent in situ hybridization of endogenous ASH1 mRNA (Takizawa et al., 1997; Trcek et al., 2012). Based on known copy numbers of core factors per cell (Trcek et al., 2012) and the stoichiometry of assembly, we estimated that a maximum of \sim 250 SHE complexes with 500 zip code binding sites exist per cell (Table S2).

Interestingly, the low protein levels of She3p limit the number of SHE complexes. We repeatedly observed that excess of She3p induces the formation of unspecific high-molecular complexes with RNA (Fig. 2 B; Müller et al., 2011). It is therefore possible that SHE complexes are limited by the availability of She3p to avoid such unspecific complexes in vivo. On the other hand, the excess of Myo4p over She3p might help to ensure that each transport particle contains two motor molecules and thus is processive.

Using published data on transcript numbers per cell (Miura et al., 2008; Nagalakshmi et al., 2008; Pelechano et al., 2010; Treek et al., 2012), we estimated that \sim 140 localizing mRNA molecules with 400-500 zip code elements are present in a dividing yeast cell (Table S1). Strikingly, these copy numbers are in very good agreement with the determined number of binding sites on SHE complexes in the cell. It suggests that the vast majority of zip code elements in the cell are bound by SHE complexes. By combining the aforementioned numbers, we calculate that multimeric SHE particles in the cell have a molecular mass between 8 and 52 MD and contain 4-25 localizing mRNAs and 7-45 SHE complexes (Fig. 5 E; see Materials and methods). Of course, not all RNAs are expressed at the same time, and some transcripts might escape binding by the SHE complex. These values do also not include accessory factor, such as translational repressors. Future work will be required to understand what features of particles with endogenous sizes and heterogeneous RNA composition are responsible for the observed motilities. One potentially important parameter to test is the endogenous actin network that might help SHE particles to move more efficiently to the bud tip.

Materials and methods

Molecular cloning

DNA fragments were produced by PCR and cloned into respective vectors using suitable restriction sites. Detailed information on plasmids, oligonucleotides, and restriction sites are given in Tables S3 and S4. For the construction of plasmid RHP169, CMD1 was amplified by PCR with primers AHO94/AHO95 and cloned into the vector pFBDM (Berger et al., 2004) with the restriction sites Xhol-Ncol. FLAG-MYO4 was amplified by PCR with primers AHO149/AHO146 and cloned into the same vector with BamHI-NotI restriction sites. The AvrII restriction site in the MYO4 coding sequence was removed by site-directed mutagenesis using the primers O209/O210, resulting in subplasmid A. SHE3-His6 was produced by PCR using the primers AHO6/O118 and cloned into pFBDM with the restriction sites BamHl-Xbal. The Spel restriction site in the coding sequence of SHE3 was removed by site-directed mutagenesis with the primers O104/O105. SHE4 was produced by PCR with the primers O213/O214 and cloned into the same vector with the restriction sites Smal-Ncol, resulting in subplasmid B. Subplasmid A was digested with Pmel-AvrII, and the resulting insert was ligated into subplasmid B previously linearized with Spel-Nrul. This step resulted in subplasmid C. MLC1 was produced by PCR with the primers O239/O240 and cloned into pFBDM with the restriction sites BamHl-Xbal, resulting in subplasmid D. Subplasmid C was digested with Pmel-AvrII, and the resulting insert was cloned into subplasmid D previously linearized with Spel-Nrul. This final step resulted in plasmid RH169 used for coexpression of all five proteins in insect cells. Point mutations in EGFP-SHE2 (N36S, R63K) were sequentially introduced via sitedirected mutagenesis. The first PCR vector amplification, using primers P21/P22 on plasmid p02 resulted in a subplasmid containing EGFP-SHE2 (N36S). The second mutagenesis step with P23/P24 finally yielded plasmid FE#22. For the production of EGFP-SHE2 (ΔhE), base pairs coding for amino acids 174-183 in She2p were deleted in plasmid p02 by using P25/P26.

Protein expression and purification

She2p, N- and C-terminal fragments of She3p, and Myo4p-C (amino acids 978-1,471) were expressed in bacteria. Full-length She3p was coexpressed with She2p wild type from baculovirus-infected insect cells and purified by multistep procedures (Müller et al., 2011). Insect cells were lysed by sonication in Ni-A1 buffer (20 mM Hepes/NaOH, pH 7.8, 500 mM NaCl, and 20 mM imidazole) and centrifuged twice at 39,000 g for 20 min. The supernatant was filtered with a 2.7-µm filter unit before loading it on a 5-ml HisTrap FF column (GE Healthcare). The bound protein was first washed with Ni-A2 buffer (20 mM Hepes/NaOH, pH 7.8, 1 M NaCl, and 40 mM imidazole) and second with Hep-A buffer (20 mM Hepes/NaOH, pH 7.8, and 200 mM NaCl). Elution was achieved by supplementing buffer Hep-A with 300 mM imidazole. Protein passed a 5-ml HiTrap Q FF column (GE Healthcare) before it was bound on a 5-ml Heparin HP column (HiTrap; GE Healthcare). Here, it was washed with 10% Hep-B buffer (20 mM Hepes/NaOH, pH 7.8, 1 M NaCl, 2 mM EDTA, and 2 mM DTT) and eluted with Hep-B buffer. Finally, She3p was loaded on a Superose 6 10/300 GL column (GE Healthcare) in a buffer that contained 20 mM Hepes/ NaOH, pH 7.8, 500 mM NaCl, and 2 mM DTT.

For motility experiments, the purification of full-length She3p was extended with an additional competition step to get completely rid of She2p wild-type remnants. Hence, She3p bound to the 5-ml HisTrap FF column was incubated with 30 µM She2p (N36S, R63K) for 15 min at 4°C during the purification. For She2p and She3p, the successful removal of contaminating nucleic acids was confirmed by measuring their absorbance at 260/280 nm. She2p and its mutants were expressed in Escherichia coli BL21 (DE3) (Niessing et al., 2004; Heuck et al., 2007; Müller et al., 2011). Cells were lysed by sonication in GST-A1 buffer (20 mM Hepes/NaOH, pH 7.5, 500 mM NaCl, 1 mM EDTA, and 2 mM DTT), supplemented with protease inhibitors. After centrifugation for 30 min at 31,000 g at 4°C, the clear lysate was loaded onto a 5-ml GSTrap FF column (GE Healthcare). The column was extensively washed with buffer GST-A1, buffer GST-A2 (buffer GST-A1 with 1 M NaCl), and buffer Q-A (10 mM Hepes/NaOH, pH 7.9, 150 mM NaCl, 1 mM EDTA, and 2 mM DTT). The protein was cleaved off the tag on the column by incubating it overnight with 20 µg/ml human rhinovirus 3C protease. She2p was then directly bound with buffer Q-A on a 5-ml HiTrap Q FF column and eluted with a gradient over 20 column volumes up to 100% buffer Q-B (10 mM Hepes/NaOH, pH 7.9, 1 M NaCl, 1 mM EDTA, and 2 mM DTT). The final purification step was SEC using a Superdex 200 16/60 GL column in SEC buffer (20 mM Hepes/NaOH, pH 7.8, 200 mM NaCl, and 2 mM DTT). It should be

noted that in contrast to a previous study (Krementsova et al., 2011) and a concurrent publication (Sladewski et al., 2013), our wild-type She2p purification involves three independent purification steps, including a washing step with high-salt buffer (see previously in this paragraph), which we consider essential to ensure removal of nucleic acid contaminations. We consider it very likely that the previously reported polydisperse behavior of wild-type She2p (Krementsova et al., 2011) was caused by nucleic acid contaminations and is not an intrinsic property of the protein itself.

Yeast calmodulin (Cmd1p) and myosin light chain (Mlc1p) were expressed in E. coli BL21 (DE3), lysed by sonication in 50 mM Tris-Cl, pH 7.5, 2 mM EDTA, and 1 mM PMSF, and centrifuged. The supernatant was boiled for 5 min, cooled, and clarified by centrifugation. For yeast calmodulin, 5 mM CaCl₂ and 1 mM DTT were added, and the protein bound to a 5-ml HiTrap Phenyl FF (high sub) column (GE Healthcare) preequilibrated with 50 mM Tris-Cl, pH 7.5, 100 mM NaCl, and 5 mM CaCl₂. The column was washed with the same buffer containing 0.1 mM CaCl₂ and then with the same low-calcium buffer with 0.5 M NaCl. Bound protein was eluted with 50 mM Tris-Cl, pH 7.5, and 1 mM EGTA and finally loaded onto a Superose 12 10/300 GL column (GE Healthcare) in complex buffer (20 mM Hepes, pH 7.8, 100 mM NaCl, 25 mM KCl, 2 mM MaCl₂, and 1 mM EGTA). For Mlc1p, the clarified supernatant was precipitated with ammonium sulfate to 80% saturation after boiling, and the protein was pelleted for 20 min at 31,000 g. The pellet was dissolved in a buffer containing 20 mM Hepes, pH 7.4, 100 mM NaCl, and 1 mM EDTA and, as the final purification step, loaded onto a Superdex 200 10/300 GL column (GE Healthcare) in motility buffer (20 mM imidazole, pH 7.4, 50 mM KCl, 4 mM MgCl₂, and 1 mM EGTA).

Calcium-ATP actin was prepared from rabbit skeletal muscle (Spudich and Watt, 1971) and purified by gel filtration on Sephacryl S-300 (GE Healthcare) in G buffer (0.2 mM ATP, 0.5 mM DTT, 0.1 mM CaCl₂, 1 mM NaN_3 , and 2 mM Tris/HCl, pH 8.0). FLAG-tagged, full-length yeast Myo4p was coexpressed with She3p, She4p, Cmd1p, and Mlc1p using the transposition system (Bac-to-Bac; Invitrogen). Recombinant baculovirus was amplified in Sf21 cells and used to infect High Five insect cells. Cells were cultured for 60–70 h. Purification of Myo4p was performed based on a previously published protocol (Krementsova et al., 2011). Cells were pelleted and resuspended in wash buffer (10 mM imidazole, pH 7.4, 300 mM NaCl, 5 mM MgCl₂, and 1 mM EGTA) supplemented by 7% (wt/vol) sucrose and protease inhibitors. After sonication, 7 µg/ml yeast Cmd1p, 7 μg/ml yeast Mlc1p, and 2 mM ATP were added, and the lysate was centrifuged twice for 20 min with 39,000 g at 4°C and filtered with a 2.7-µm filter. The cleared lysate was incubated with anti-FLAG M2 affinity gel resin (Sigma-Aldrich) for 1 h at 4°C, and the resin was washed with wash buffer. Bound protein was eluted with 0.15 mg/ml FLAG peptide in wash buffer. The eluate was dialyzed in motility buffer (25 mM imidazole, pH 7.4, 50 mM KCl, 4 mM MgCl₂, and 1 mM EGTA) supplemented with 2 mM DTT followed by dialysis in motility buffer supplemented with 2 mM DTT and 50% (vol/vol) glycerol and storage at -20°C. Mass spectrometric analysis showed that She3p, She4p, Cmd1p, and Mlc1p were copurified with full-length Myo4p. All components except for She4p were present in the expected amounts as judged by SDS-PAGE. The preparation was active in actin gliding assays.

RNA preparation

RNAs were produced by chemical synthesis, in vitro transcription, or expression in *E. coli* (Table S5; Edelmann et al., 2013). In vitro transcribed RNAs were produced with the MEGAshortscript kit (Ambion) and purified by native PAGE or by phenol extraction and isopropanol precipitation. RNAs for tRNA tagging were fused to the *E. coli* initiator tRNA(Met), expressed in *E. coli* JM101 cells (New England Biolabs, Inc.), and purified by ion exchange chromatography (Ponchon et al., 2009; Müller et al., 2011). In brief, the harvested bacterial cell pellet was dissolved in a buffer containing 10 mM Tris/HCl, pH 7.4, and 10 mM magnesium acetate. RNA was recovered by phenolic extraction and ethanol precipitation. The resulting pellet was dissolved in 40 mM sodium phosphate buffer, pH 7.0, and loaded on a MonoQ 5/50 GL column (GE Healthcare). After washing with the same buffer containing 450 mM NaCl, RNA was eluted with a shallow gradient over 30 column volumes up to 650 mM NaCl. Finally, RNA was ethanol precipitated.

Chemical cross-linking of proteins

In a total volume of 22 µl, 1–10 µM She3p or Myo4p was incubated with 45 mM EDC and 45 mM NHS in a buffer containing 20 mM Hepes/NaOH, pH 7.8, and 500 mM NaCl for 20 min at 25°C. Afterward, the samples were analyzed by SDS-PAGE and Coomassie blue staining.

Analytical SEC

Analytical SEC was performed at 4°C using a Superose 6 10/300 GL column in HNMD buffer (20 mM Hepes, pH 7.8, 200 mM NaCl, 2 mM MgCl₂, and 2 mM DTT). Fractions were analyzed by SDS-PAGE with Coomassie blue staining and PAGE with GelRed staining (Biotium).

Dynamic light scattering and density gradient centrifugation of SHE core complexes

In a total volume of 100 μI , the SHE core complex was reconstituted with 30 μM She2p, 30 μM She3p, 15 μM Myo4p-C, and 15 μM zip code RNA (7.5 µM in the case of 2× ASH1-E3-77-tRNA). Samples were analyzed by dynamic light scattering with a dynamic light scattering instrument (Viscotek 802; Malvern) at 20°C. All samples showed one major species (>95% intensity), whose hydrodynamic radius is indicated. Volumes of particles were calculated by assuming an idealized globular particle sphere $(V = 4/3 \times \pi r^3)$. Using the hydrodynamic radii from dynamic light scattering experiments (hydrodynamic radius [Rh] = 18.1 nm for particles not multimerized by RNA and Rh = 86.4 nm for particles cross-linked by RNA with two zip code elements), a difference in volume of 109-fold was calculated. After dynamic light scattering, the samples were loaded on 5-30% sucrose gradients in HNMD buffer and separated by ultracentrifugation (182,000 gfor 15 h and 30 min at 4°C; SW40 Ti rotor; Beckman Coulter). Fractions were collected from the bottom to the top of the gradient using a peristaltic pump and analyzed by SDS-PAGE with Coomassie blue staining and agarose gel electrophoresis with GelRed staining.

SL

SLS was performed with a triple detector array (Viscotek TDA 305) coupled to a liquid chromatography system (ÄKTApurifier 10; GE Healthcare). The system was calibrated with 3.5 mg/ml BSA. Respective proteins and RNA were mixed with a stoichiometric or near-stoichiometric ratio at a total concentration of 1–5 mg/ml, and 100 µl thereof was separated on a SEC column at 4°C with a flow rate of 0.5 ml/min. For Myo4p-C and for the She3p:Myo4p-C complex, a Superdex 200 10/300 GL column in SLS buffer (20 mM Hepes/NaOH, pH 7.8, 200 mM NaCl, and 1 mM Tris(2carboxyethyl)phosphine hydrochloride) was used. All other samples were analyzed on a Superose 6 10/300 GL column in HNMD buffer. The molecular mass of the sample was determined from the light scattering at right angle, the refractive index, and the refractive index increment (dn/dc). A dn/dc value of 0.185 ml/g was used for proteins, and a value of 0.170 ml/g was used for RNA (Rambo and Doudna, 2004). For RNA/protein complexes, the dn/dc value was calculated according to the mass fraction of protein and RNA in the complex. Thus, a dn/dc value of 0.182 ml/g was used for ASH1-E3-51:She2p and ASH1-E3-77-tRNA:She2p:She3: Myo4p-C. For tRNA-tagged zip code RNAs in complex with She2p, a dn/dc value of 0.178 was used. Data analysis was performed with the OmniSEC software (Malvern).

Isothermal titration calorimetry

Experiments were performed with an isothermal titration calorimeter (iTC200; GE Healthcare) at 20°C in 20 mM Hepes/NaOH, pH 7.8, 500 mM NaCl, and 1 mM Tris(2-carboxyethyl)phosphine hydrochloride. A concentration of 10 µM Myo4p-C was used in the measuring cell and titrated with 220 µM She3p. The data were corrected for She3p titration into buffer. The number of binding sites (n), the association constant (K_a), and the change in enthalpy (Δ H) were obtained by fitting the data with the one-site binding model included in the MicroCal data analysis package based on the program Origin (OriginLab). The experiment was performed as a duplicate.

EMSA

EMSAs were performed based on previous protocols (Graebsch et al., 2009; Müller et al., 2011). In a 20-ml reaction, the protein was incubated with 5 nM 32 P-labeled RNA oligonucleotide in HNMD buffer (20 mM Hepes, pH 7.8, 200 mM NaCl, 2 mM MgCl $_2$, and 2 mM DTT) supplemented with 4% (vol/vol) glycerol and 30 mg/ml yeast tRNA for 20 min at 20°C. Protein–RNA complexes were resolved by PAGE (native 4% gel in 0.5x TBE (Tris-borate-EDTA) running buffer at 90 V for 45 min at 20°C). Unlabeled RNA was added at the indicated concentration for stoichiometry determination.

Quantitative mass spectrometry

Complexes were reconstituted and purified by SEC in HNMD buffer (SHE complexes) or in SLS buffer (She3p:Myo4p complex). Care was taken that the complexes were saturated with all components. 1–3 µg of the purified complex were incubated with 50 mM DTT for 60 min at room temperature followed by treatment with 10 mM iodoacetamide for 30 min at room temperature. Heavy isotope-labeled peptides (SpikeTides_TQL; JPT Peptide

Technologies) were dissolved in 40 mM ammonium bicarbonate. In a total volume of 50 μ l, the pretreated sample was mixed with 0.5 pmol/ μ l of each peptide, and the mixture was digested with 0.8 μ g trypsin overnight at 37°C. 10 μ l thereof (5 pmol of each heavy isotope-labeled peptide) was analyzed by nano-liquid chromatography-electrospray ionization-tandem mass spectrometry. Heavy and native light peptides were identified by search in a homemade database. The ratio of the peak areas in the mass spectrometry scan was used to determine the amount of the respective light peptides in the sample. The peptide sequences were as follows: She3p peptide (residues 45–58), VIESLHDQIDMLTK*-Z; and Myo4p peptide (residues 1,445–1,464), YDTSAITQNSNTEGLATVSK*-Z (asterisks mark amino acids labeled with the heavy isotopes 15 N and 13 C. Z marks the cleavable JPT tag).

Single-molecule motility assay

Single-molecule motility experiments were designed on the basis of previously described conditions (Krementsova et al., 2011).

F-actin preparation. Fluorescent actin filaments were prepared with 5 μM of purified rabbit G-actin (containing 10% tetramethylrhodamine [TMR]-labeled actin), polymerized in actin buffer (25 mM imidazole, pH 7.4, 25 mM KCl, 4 mM MgCl₂, 1 mM EGTA, and 10 mM DTT) for 1 h at room temperature, and stabilized with equimolar amounts of phalloidin (Sigma-Aldrich).

Flow cell preparation. 15-µl flow cells (area 18×3 mm) covered by a nitrocellulose coverslip were used. Flow cells were preincubated with 0.1 mg/ml Nethyl maleimide—modified heavy meromyosin (Meeusen and Cande, 1979) in 25 mM imidazole, pH 7.4, 300 mM KCl, 4 mM MgCl₂, 1 mM EgA, and 10 mM DTT for 3 min, rinsed with 1 mg/ml BSA in H₂O, incubated with fluorescently labeled F-actin in actin buffer for 5 min, and rinsed twice with motility buffer (25 mM imidazole, pH 7.4, 50 mM KCl, 4 mM MgCl₂, and 1 mM EGTA) supplemented with 1 mg/ml BSA and 10 mM DTT.

Preparation and labeling of complexes. For RNA detection in TIRFM experiments, in which both fluorescently labeled *ASH1-3'* and *IST2* RNA were used, *ASH1-E3-77* was hybridized with Cy3.5-labeled and *IST2* with Atto488-labeled antisense DNA oligonucleotides. For this, hybridization was performed in a thermocycler at 90°C for 1 min followed by an incubation at 37°C for 5 min and a final incubation step on ice for 5 min.

For TIRFM experiments with unlabeled RNA, 200 nM GFP-She2p and 100 nM RNA were premixed with 200 nM She3p and ~100 nM Myo4p (Myo4p preparation also contained copurified She3p, She4p, Cmd1p, and Mlc1p) in motility buffer supplemented with 2 mM DTT. For experiments with labeled ASH1-E3-77 and IST2 RNA, a premix containing 200 nM She2p, 200 nM She3p, 100 nM Myo4p, 80 nM IST2, and 60 nM ASH1-E3-77 was made as outlined in this paragraph. Before infusion into the flow cell, the premix was diluted 1:100 in motility buffer containing 0.2 mg/ml Cmd1p, 0.2 mg/ml Mlc1p, 1 mg/ml BSA, 10 mM DTT, 1% (wi/vol) glucose, oxygen scavenging system (1,700 U/ml catalase and 26 U/ml glucose oxidase), 0.4 mg/ml glucose, and 2 mM ATP, yielding approximate final concentrations of 2 nM GFP-She2p, 2 nM She3p, 1 nM Myo4p, and 1 nM RNA. For experiments with labeled ASH1-E3-77 and IST2 RNA, the approximate final concentrations were 7 nM She2p, 7 nM She3p, 3.5 nM Myo4p, 2.8 nM IST2, and 2.1 nM ASH1-E3-77 RNA.

Data acquisition. A TIRF microscope (IX50; Olympus) equipped with a Plan apochromatic objective lens (100x, NA 1.45 oil) and linked to an electron-multiplying charge-coupled device camera (iXon Plus X-4818; Andor Technology) along with the vendor's IQ software (version 1.10.2; Andor Technology) was used. During the actual acquisition, a Perfect Focus System MS-200 (Applied Scientific Instrumentation) that was controlled via ASI software (version 1.6b; Applied Scientific Instrumentation) was used. Fluorophore excitation at 488 and 561 nm was performed with low-power continuous wave lasers (Sapphire; Coherent). Image acquisition took place for 3–10 min, at 110-ms exposure and 250-ms cycle time and room temperature. For photobleaching experiments on Myo4p:GFP-She2p:She3p: RNA particles as well as GFP-She2p alone, fluorophores were excited by the 488-nm laser while acquiring every 55 ms without actually operating the laser beam shutter. Typically, image sequences of 2–3 min were taken.

Image and data analysis. Only directional uninterrupted (i.e., no stopping) motility events of individual complexes of similar fluorescence intensity, which lasted longer than 1 s were considered for the analysis. Subsequently, potential extreme values (outliers) were identified by plotting the obtained raw data as box—whisker plots. An outlier was defined as such when its percentile was <2.5 or >100. To ensure statistical quality and relevance, the final data herein presented do not contain said outliers. To ensure that no protein aggregates are included in the analysis, events occurring after 8 min (after diluting in motility buffer plus ATP and

oxygen-scavenging system) were not considered. For the photobleaching analysis of processively moving events, in ImageJ (National Institutes of Health), image sequences were background corrected by using a 6 \times 6–pixel window. Mean integrated intensities over time were determined for each consecutive frame.

Run lengths and velocities were obtained from a single exponential fit (Miura et al., 2008) and a Gaussian fit (y = a × exp × {-[(x - x₀)/b]²}) to the respective distributions. Distances of single displacements were measured by brightest centroid tracking, using MTrackJ for ImageJ. Data plotting and fitting, as well as the statistical analysis, were performed with Igor Pro software (WaveMetrics). Run frequencies were generated by dividing the total number of processive runs by the total F-actin length, time, and final myosin concentration.

Calculation of particle number and size

Our calculation is based on two previous observations in vivo: one transport particle contains between 2.4 and 15.6 (mean: 7.2) ASH1 mRNAs (Haim et al., 2007), and \sim 88 ASH1 mRNAs are present in a dividing yeast cell (Trcek et al., 2012). From these numbers, we calculated the number of particles per cell by dividing the number of ASH1 mRNAs per cell by the minimal/maximal/mean number of ASH1mRNAs per particle. We estimated that 142 localizing mRNAs are present per dividing yeast cell (Table S1) and divided this number by the number of particles per cell to obtain the number of mRNAs per particle. Using the stoichiometry of the SHE complex determined in this study, we estimated that a maximum of 252 SHE complexes could be formed in one cell (Table S2). This number was derived from the reported protein copy number of 1,010 for She3p (Ghaemmaghami et al., 2003), which is limiting for SHE complex formation. By dividing the number of SHE complexes per cell by the number of particles per cell, we obtained the number of SHE complexes per particle. We determined the molecular mass of the particles by dividing the molecular mass of all SHE complexes and localizing mRNAs in one cell (Table S2) by the number of particles per cell.

Online supplemental material

Fig. S1 shows stoichiometry determination of the SHE subcomplex by SEC and chemical cross-linking. Fig. S2 shows control EMSAs for stoichiometry determination of the mature SHE complex. Fig. S3 shows stoichiometry determination of the mature SHE complex by SEC. Fig. S4 shows results from bleaching experiments. In Fig. S5, motile events per micrometer actin and time from different SHE particles are compared. Video 1 shows single-particle motility of a SHE complex consisting of ASH1-3' + GFP-She2p + She3p + Myo4p. Video 2 shows single-particle motility of a SHE complex consisting of GFP-She2p + She3p + Myo4p. Video 3 shows single-particle motility of a SHE complex consisting of GFP-She2p(N36S, R63K) + She3p + Myo4p. Video 4 shows single-particle motility of a SHE complex consisting of ASH1-3' + GFP-She2p (ΔhE) + She3p + Myo4p. Video 5 shows single-particle motility of a SHE complex consisting of (2x E3-77-tRNA) + GFP-She2p + She3p + Myo4p. Video 6 shows single-particle motility of a SHE complex consisting of Cy3.5-ASH1-3' + Atto488-IST2 + She2p + She3p + Myo4p. Table S1 shows the mRNAs that have been reported as being transported in a She2p-dependent manner. Table S2 shows an estimate of SHE complexes per cell. Table S3 shows all plasmids used in this study. Table S4 shows all DNA oligonucleotides used in this study. Table S5 lists RNA sequences used in this study. Online supplemental material is available at http://www.jcb.org/cgi/content/full/jcb.201302095/DC1. Additional data are available in the JCB DataViewer at http://dx.doi.org/10.1083/ jcb.201302095.dv.

We are grateful to Annika Niedner, Sigrun Jaklin, and Arie Geerlof for their support. We acknowledge the technical support by the Protein Expression and Purification Facility of the Helmholtz Zentrum München.

This work was supported by the Deutsche Forschungsgemeinschaft (FOR855 and SFB646 to D. Niessing and SFB863 to Z. Ökten). Research reported in this publication was supported by the National Center for Advancing Translational Sciences of the National Institutes of Health (under award number UL1TR000430 to D.R. Kovar) as well as a grant from the Human Frontier Science Program Young Investigator Program (under award number RGY0071/2011 to D.R. Kovar).

Submitted: 19 February 2013 Accepted: 15 November 2013

References

- Amrute-Nayak, M., and S.L. Bullock. 2012. Single-molecule assays reveal that RNA localization signals regulate dynein-dynactin copy number on individual transcript cargoes. *Nat. Cell Biol.* 14:416–423. http://dx.doi .org/10.1038/ncb2446
- Aronov, S., R. Gelin-Licht, G. Zipor, L. Haim, E. Safran, and J.E. Gerst. 2007. mRNAs encoding polarity and exocytosis factors are cotransported with the cortical endoplasmic reticulum to the incipient bud in Saccharomyces cerevisiae. Mol. Cell. Biol. 27:3441–3455. http://dx.doi .org/10.1128/MCB.01643-06
- Beach, D.L., E.D. Salmon, and K. Bloom. 1999. Localization and anchoring of mRNA in budding yeast. Curr. Biol. 9:569–578. http://dx.doi.org/ 10.1016/S0960-9822(99)80260-7
- Berger, I., D.J. Fitzgerald, and T.J. Richmond. 2004. Baculovirus expression system for heterologous multiprotein complexes. *Nat. Biotechnol.* 22:1583–1587. http://dx.doi.org/10.1038/nbt1036
- Bertrand, E., P. Chartrand, M. Schaefer, S.M. Shenoy, R.H. Singer, and R.M. Long. 1998. Localization of ASH1 mRNA particles in living yeast. Mol. Cell. 2:437–445. http://dx.doi.org/10.1016/S1097-2765(00)80143-4
- Besse, F., S. López de Quinto, V. Marchand, A. Trucco, and A. Ephrussi. 2009. Drosophila PTB promotes formation of high-order RNP particles and represses oskar translation. Genes Dev. 23:195–207. http://dx.doi.org/10.1101/gad.505709
- Bobola, N., R.P. Jansen, T.H. Shin, and K. Nasmyth. 1996. Asymmetric accumulation of Ash1p in postanaphase nuclei depends on a myosin and restricts yeast mating-type switching to mother cells. *Cell*. 84:699–709. http://dx.doi.org/10.1016/S0092-8674(00)81048-X
- Böhl, F., C. Kruse, A. Frank, D. Ferring, and R.P. Jansen. 2000. She2p, a novel RNA-binding protein tethers ASH1 mRNA to the Myo4p myosin motor via She3p. EMBO J. 19:5514–5524. http://dx.doi.org/10.1093/ emboj/19.20.5514
- Bookwalter, C.S., M. Lord, and K.M. Trybus. 2009. Essential features of the class V myosin from budding yeast for ASH1 mRNA transport. *Mol. Biol. Cell.* 20:3414–3421. http://dx.doi.org/10.1091/mbc.E08-08-0801
- Chartrand, P., X.H. Meng, R.H. Singer, and R.M. Long. 1999. Structural elements required for the localization of ASH1 mRNA and of a green fluorescent protein reporter particle in vivo. Curr. Biol. 9:333–336. http://dx.doi.org/10.1016/S0960-9822(99)80144-4
- Chartrand, P., X.H. Meng, S. Hüttelmaier, D. Donato, and R.H. Singer. 2002. Asymmetric sorting of ash1p in yeast results from inhibition of translation by localization elements in the mRNA. *Mol. Cell.* 10:1319–1330. http://dx.doi.org/10.1016/S1097-2765(02)00694-9
- Chung, S., and P.A. Takizawa. 2010. Multiple Myo4 motors enhance ASH1 mRNA transport in Saccharomyces cerevisiae. J. Cell Biol. 189:755–767. http://dx.doi.org/10.1083/jcb.200912011
- Du, T.G., S. Jellbauer, M. Müller, M. Schmid, D. Niessing, and R.P. Jansen. 2008. Nuclear transit of the RNA-binding protein She2 is required for translational control of localized ASH1 mRNA. EMBO Rep. 9:781–787. http://dx.doi.org/10.1038/embor.2008.112
- Dunn, B.D., T. Sakamoto, M.S. Hong, J.R. Sellers, and P.A. Takizawa. 2007. Myo4p is a monomeric myosin with motility uniquely adapted to transport mRNA. J. Cell Biol. 178:1193–1206. http://dx.doi.org/10.1083/jcb.200707080
- Edelmann, F.T., A. Niedner, and D. Niessing. 2013. Production of pure and functional RNA for in vitro reconstitution experiments. *Methods*.
- Ghaemmaghami, S., W.K. Huh, K. Bower, R.W. Howson, A. Belle, N. Dephoure, E.K. O'Shea, and J.S. Weissman. 2003. Global analysis of protein expression in yeast. *Nature*. 425:737–741. http://dx.doi.org/10.1038/nature02046
- Gonzalez, I., S.B. Buonomo, K. Nasmyth, and U. von Ahsen. 1999. ASH1 mRNA localization in yeast involves multiple secondary structural elements and Ash1 protein translation. Curr. Biol. 9:337–340. http://dx.doi .org/10.1016/S0960-9822(99)80145-6
- Graebsch, A., S. Roche, and D. Niessing. 2009. X-ray structure of Pur-alpha reveals a Whirly-like fold and an unusual nucleic-acid binding surface. *Proc. Natl. Acad. Sci. USA*. 106:18521–18526. http://dx.doi.org/10 .1073/pnas.0907990106
- Haim, L., G. Zipor, S. Aronov, and J.E. Gerst. 2007. A genomic integration method to visualize localization of endogenous mRNAs in living yeast. *Nat. Methods*. 4:409–412.
- Heuck, A., T.G. Du, S. Jellbauer, K. Richter, C. Kruse, S. Jaklin, M. Müller, J. Buchner, R.P. Jansen, and D. Niessing. 2007. Monomeric myosin V uses two binding regions for the assembly of stable translocation complexes. Proc. Natl. Acad. Sci. USA. 104:19778–19783. http://dx.doi.org/10.1073/pnas.0706780104
- Heuck, A., I. Fetka, D.N. Brewer, D. Hüls, M. Munson, R.P. Jansen, and D. Niessing. 2010. The structure of the Myo4p globular tail and its function

- in ASH1 mRNA localization. J. Cell Biol. 189:497–510. http://dx.doi.org/10.1083/jcb.201002076
- Heym, R.G., and D. Niessing. 2012. Principles of mRNA transport in yeast. Cell. Mol. Life Sci. 69:1843–1853. http://dx.doi.org/10.1007/s00018-011-0902-4
- Hodges, A.R., E.B. Krementsova, and K.M. Trybus. 2008. She3p binds to the rod of yeast myosin V and prevents it from dimerizing, forming a singleheaded motor complex. *J. Biol. Chem.* 283:6906–6914. http://dx.doi.org/10 .1074/jbc.M708865200
- Hogan, D.J., D.P. Riordan, A.P. Gerber, D. Herschlag, and P.O. Brown. 2008. Diverse RNA-binding proteins interact with functionally related sets of RNAs, suggesting an extensive regulatory system. *PLoS Biol.* 6:e255. http://dx.doi.org/10.1371/journal.pbio.0060255
- Jambhekar, A., K. McDermott, K. Sorber, K.A. Shepard, R.D. Vale, P.A. Takizawa, and J.L. DeRisi. 2005. Unbiased selection of localization elements reveals cis-acting determinants of mRNA bud localization in Saccharomyces cerevisiae. Proc. Natl. Acad. Sci. USA. 102:18005–18010. http://dx.doi.org/10.1073/pnas.0509229102
- Jansen, R.P., and D. Niessing. 2012. Assembly of mRNA-protein complexes for directional mRNA transport in eukaryotes—an overview. Curr. Protein Pept. Sci. 13:284–293. http://dx.doi.org/10.2174/138920312801619493
- Jansen, R.P., C. Dowzer, C. Michaelis, M. Galova, and K. Nasmyth. 1996. Mother cell-specific HO expression in budding yeast depends on the unconventional myosin myo4p and other cytoplasmic proteins. *Cell.* 84:687–697. http://dx.doi.org/10.1016/S0092-8674(00)81047-8
- Krementsova, E.B., A.R. Hodges, C.S. Bookwalter, T.E. Sladewski, M. Travaglia, H.L. Sweeney, and K.M. Trybus. 2011. Two single-headed myosin V motors bound to a tetrameric adapter protein form a processive complex. J. Cell Biol. 195:631–641. http://dx.doi.org/10.1083/jcb.201106146
- Kruse, C., A. Jaedicke, J. Beaudouin, F. Böhl, D. Ferring, T. Güttler, J. Ellenberg, and R.P. Jansen. 2002. Ribonucleoprotein-dependent localization of the yeast class V myosin Myo4p. J. Cell Biol. 159:971–982. http://dx.doi.org/10.1083/jcb.200207101
- Lange, S., Y. Katayama, M. Schmid, O. Burkacky, C. Bräuchle, D.C. Lamb, and R.P. Jansen. 2008. Simultaneous transport of different localized mRNA species revealed by live-cell imaging. *Traffic*. 9:1256–1267. http://dx.doi .org/10.1111/j.1600-0854.2008.00763.x
- Lescoute, A., and E. Westhof. 2006. Topology of three-way junctions in folded RNAs. RNA. 12:83–93. http://dx.doi.org/10.1261/rna.2208106
- Li, J.F., and A. Nebenführ. 2008. The tail that wags the dog: the globular tail domain defines the function of myosin V/XI. *Traffic*. 9:290–298. http:// dx.doi.org/10.1111/j.1600-0854.2007.00687.x
- Long, R.M., R.H. Singer, X. Meng, I. Gonzalez, K. Nasmyth, and R.P. Jansen. 1997. Mating type switching in yeast controlled by asymmetric localization of ASHI mRNA. Science. 277:383–387. http://dx.doi.org/10.1126/science.277.5324.383
- Long, R.M., W. Gu, E. Lorimer, R.H. Singer, and P. Chartrand. 2000. She2p is a novel RNA-binding protein that recruits the Myo4p-She3p complex to ASHI mRNA. EMBO J. 19:6592–6601. http://dx.doi.org/10.1093/emboj/ 19.23.6592
- Marchand, V., I. Gaspar, and A. Ephrussi. 2012. An intracellular transmission control protocol: assembly and transport of ribonucleoprotein complexes. Curr. Opin. Cell Biol. 24:202–210. http://dx.doi.org/10.1016/j.ceb.2011.12.014
- Martin, K.C., and A. Ephrussi. 2009. mRNA localization: gene expression in the spatial dimension. *Cell*. 136:719–730. http://dx.doi.org/10.1016/j.cell 2009.01.044
- Meeusen, R.L., and W.Z. Cande. 1979. N-ethylmaleimide-modified heavy meromyosin. A probe for actomyosin interactions. J. Cell Biol. 82:57–65. http://dx.doi.org/10.1083/jcb.82.1.57
- Miura, F., N. Kawaguchi, M. Yoshida, C. Uematsu, K. Kito, Y. Sakaki, and T. Ito. 2008. Absolute quantification of the budding yeast transcriptome by means of competitive PCR between genomic and complementary DNAs. BMC Genomics. 9:574. http://dx.doi.org/10.1186/1471-2164-9-574
- Müller, M., K. Richter, A. Heuck, E. Kremmer, J. Buchner, R.P. Jansen, and D. Niessing. 2009. Formation of She2p tetramers is required for mRNA binding, mRNP assembly, and localization. RNA. 15:2002–2012. http://dx.doi.org/10.1261/rna.1753309
- Müller, M., R.G. Heym, A. Mayer, K. Kramer, M. Schmid, P. Cramer, H. Urlaub, R.P. Jansen, and D. Niessing. 2011. A cytoplasmic complex mediates specific mRNA recognition and localization in yeast. *PLoS Biol.* 9:e1000611. http://dx.doi.org/10.1371/journal.pbio.1000611
- Nagalakshmi, U., Z. Wang, K. Waern, C. Shou, D. Raha, M. Gerstein, and M. Snyder. 2008. The transcriptional landscape of the yeast genome defined by RNA sequencing. *Science*. 320:1344–1349. http://dx.doi .org/10.1126/science.1158441
- Niessing, D., S. Hüttelmaier, D. Zenklusen, R.H. Singer, and S.K. Burley. 2004. She2p is a novel RNA binding protein with a basic helical hairpin motif. Cell. 119:491–502. http://dx.doi.org/10.1016/j.cell.2004.10.018

- Oeffinger, M., K.E. Wei, R. Rogers, J.A. DeGrasse, B.T. Chait, J.D. Aitchison, and M.P. Rout. 2007. Comprehensive analysis of diverse ribonucleoprotein complexes. *Nat. Methods*. 4:951–956. http://dx.doi.org/10.1038/nmeth1101
- Olivier, C., G. Poirier, P. Gendron, A. Boisgontier, F. Major, and P. Chartrand. 2005. Identification of a conserved RNA motif essential for She2p recognition and mRNA localization to the yeast bud. *Mol. Cell. Biol.* 25:4752–4766. http://dx.doi.org/10.1128/MCB.25.11.4752-4766.2005
- Pelechano, V., S. Chávez, and J.E. Pérez-Ortín. 2010. A complete set of nascent transcription rates for yeast genes. PLoS ONE. 5:e15442. http://dx.doi .org/10.1371/journal.pone.0015442
- Ponchon, L., and F. Dardel. 2007. Recombinant RNA technology: the tRNA scaffold. Nat. Methods. 4:571–576. http://dx.doi.org/10.1038/nmeth1058
- Ponchon, L., G. Beauvais, S. Nonin-Lecomte, and F. Dardel. 2009. A generic protocol for the expression and purification of recombinant RNA in *Escherichia coli* using a tRNA scaffold. *Nat. Protoc.* 4:947–959. http:// dx.doi.org/10.1038/nprot.2009.67
- Rambo, R.P., and J.A. Doudna. 2004. Assembly of an active group II intronmaturase complex by protein dimerization. *Biochemistry*. 43:6486–6497. http://dx.doi.org/10.1021/bi049912u
- Reck-Peterson, S.L., M.J. Tyska, P.J. Novick, and M.S. Mooseker. 2001. The yeast class V myosins, Myo2p and Myo4p, are nonprocessive actin-based motors. J. Cell Biol. 153:1121–1126. http://dx.doi.org/10.1083/jcb.153.5.1121
- Shen, Z., A. St-Denis, and P. Chartrand. 2010. Cotranscriptional recruitment of She2p by RNA pol II elongation factor Spt4-Spt5/DSIF promotes mRNA localization to the yeast bud. *Genes Dev.* 24:1914–1926. http://dx.doi.org/10.1101/gad.1937510
- Shepard, K.A., A.P. Gerber, A. Jambhekar, P.A. Takizawa, P.O. Brown, D. Herschlag, J.L. DeRisi, and R.D. Vale. 2003. Widespread cytoplasmic mRNA transport in yeast: identification of 22 bud-localized transcripts using DNA microarray analysis. *Proc. Natl. Acad. Sci. USA*. 100:11429–11434. http://dx.doi.org/10.1073/pnas.2033246100
- Sil, A., and I. Herskowitz. 1996. Identification of asymmetrically localized determinant, Ash1p, required for lineage-specific transcription of the yeast HO gene. Cell. 84:711–722. http://dx.doi.org/10.1016/S0092-8674(00)81049-1
- Sladewski, T.E., C.S. Bookwalter, M.S. Hong, and K.M. Trybus. 2013. Single-molecule reconstitution of mRNA transport by a class V myosin. *Nat. Struct. Mol. Biol.* 20:952–957. http://dx.doi.org/10.1038/nsmb.2614
- Spudich, J.A., and S. Watt. 1971. The regulation of rabbit skeletal muscle contraction. I. Biochemical studies of the interaction of the tropomyosin-troponin complex with actin and the proteolytic fragments of myosin. J. Biol. Chem. 246:4866–4871.
- Takizawa, P.A., A. Sil, J.R. Swedlow, I. Herskowitz, and R.D. Vale. 1997. Actin-dependent localization of an RNA encoding a cell-fate determinant in yeast. *Nature*. 389:90–93. http://dx.doi.org/10.1038/38015
- Takizawa, P.A., J.L. DeRisi, J.E. Wilhelm, and R.D. Vale. 2000. Plasma membrane compartmentalization in yeast by messenger RNA transport and a septin diffusion barrier. *Science*. 290:341–344. http://dx.doi .org/10.1126/science.290.5490.341
- Trcek, T., J.A. Chao, D.R. Larson, H.Y. Park, D. Zenklusen, S.M. Shenoy, and R.H. Singer. 2012. Single-mRNA counting using fluorescent in situ hybridization in budding yeast. *Nat. Protoc.* 7:408–419. http://dx.doi.org/10.1038/nprot.2011.451
- Trybus, K.M. 2008. Myosin V from head to tail. *Cell. Mol. Life Sci.* 65:1378–1389. http://dx.doi.org/10.1007/s00018-008-7507-6

Heym et al., http://www.jcb.org/cgi/content/full/jcb.201302095/DC1

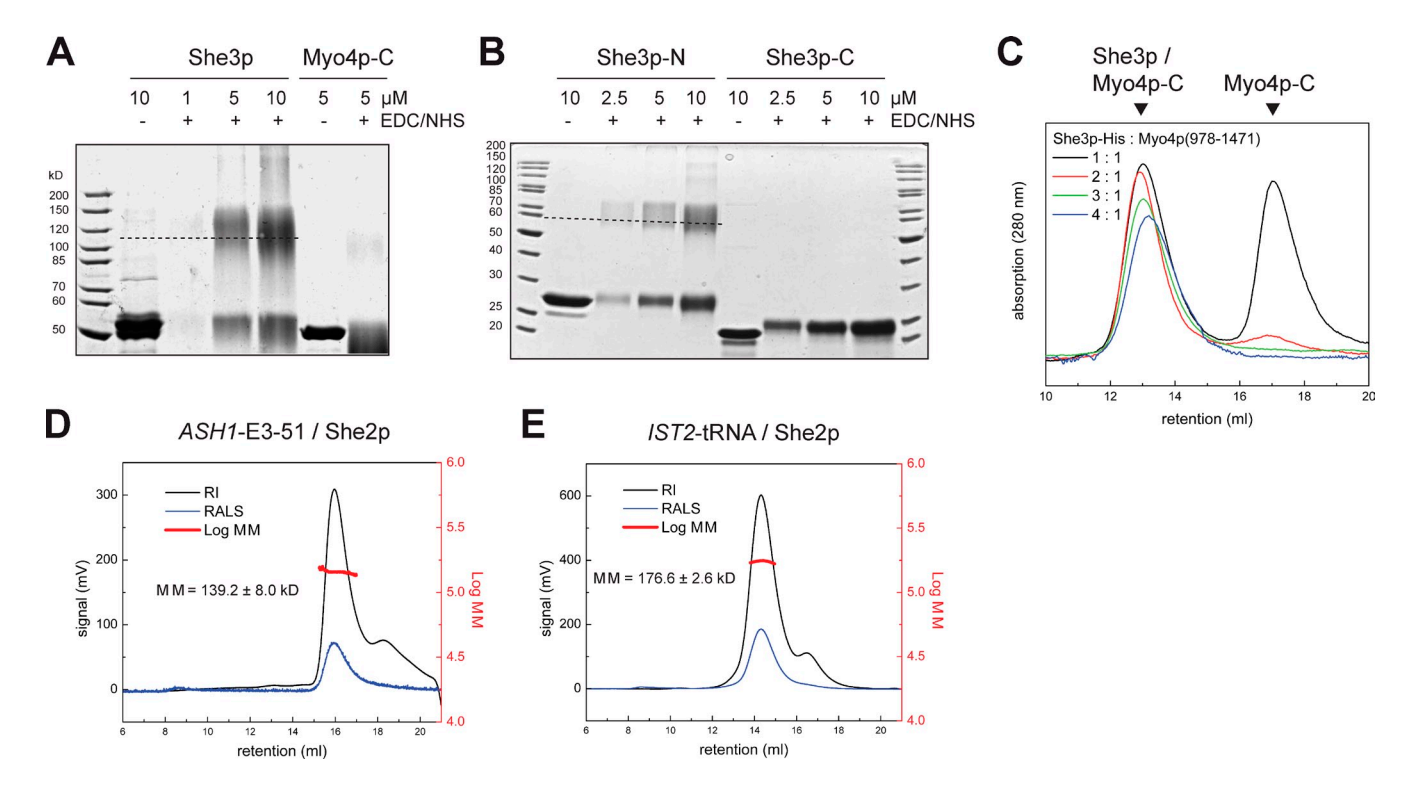


Figure S1. Assessment of SHE subcomplexes. (A) Chemical cross-linking experiments with the She3p:Myo4p complex. Cross-linking with EDC and NHS revealed oligomerization of full-length She3p. After cross-linking, samples were subjected to SDS-PAGE and Coomassie blue protein staining. The monomeric Myo4p-C was not cross-linking of N- and C-terminal fragments of She3p demonstrated that only the N terminus mediates oligomerization. The dotted line indicates the expected migration of the dimeric She3p N terminus. (C) Stoichiometry determination of the She3p:Myo4p complex by SEC. Increasing amounts of Myo4p-C (3–12 µM) were mixed with a constant amount of She3p (12 µM). Excess Myo4p-C was separated from the complex by SEC. The complex was saturated at a ratio of two molecules She3p to one molecule Myo4p-C. (D and E) SLS of She2p:RNA complexes. She2p tetramer binds two RNA zip code elements. SLS profiles of the ASH1-E3-51:She2p complex (D) and the IST2-tRNA:She2p complex (E). The molecular mass measurements for these complexes were less accurate than for the ASH1-T7-tRNA (Fig. 1 E and Table 1), which is likely caused by lower complex stability and partial dissociation during chromatography. Note that a slight excess of ASH1-E3-51 was used to saturate the complex. RI, refractive index; RALS, right angle light scattering; MM, fitted molecular mass.

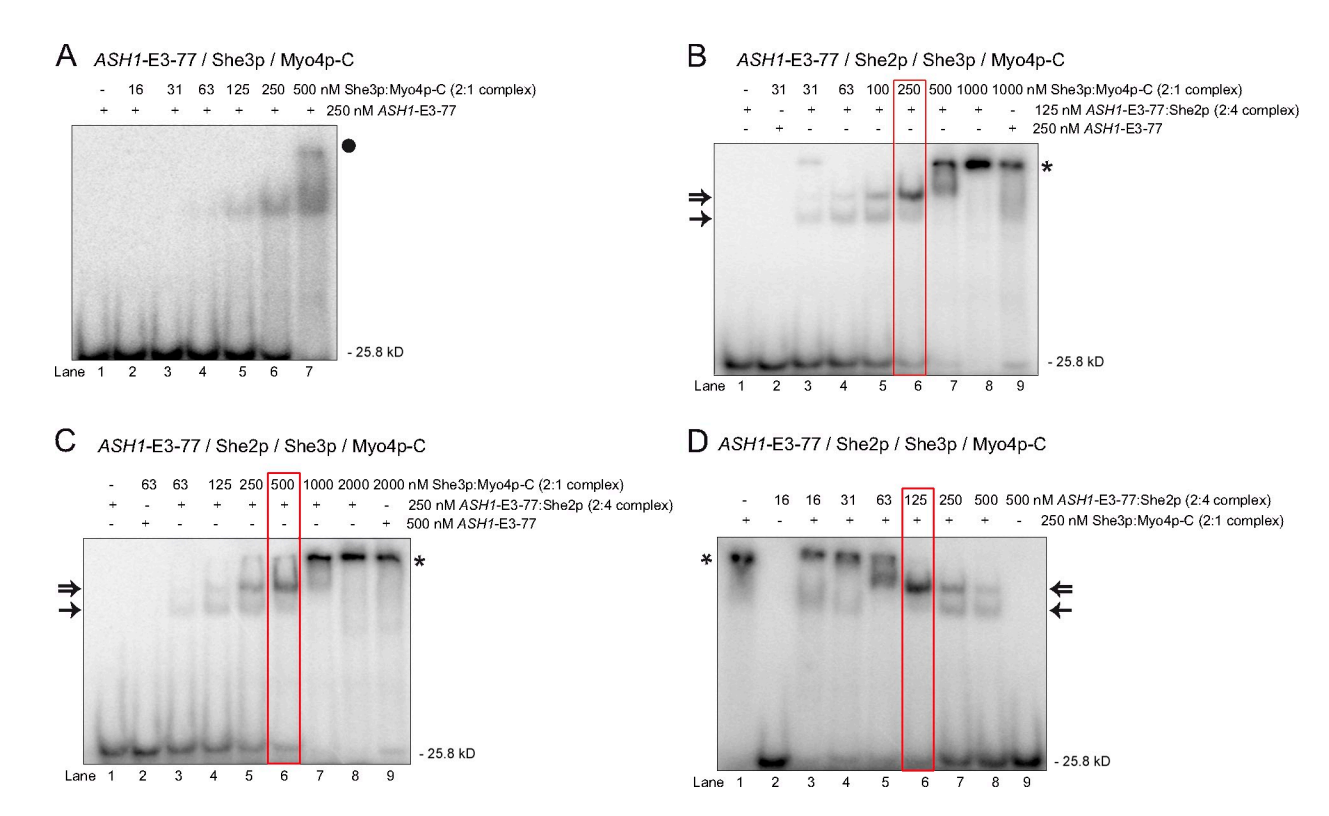


Figure S2. Control EMSAs for the stoichiometry determination of the SHE core complex. (A) Control EMSA with She3p:Myo4p-C and ASH1-E3 RNA. No significant formation of high-molecular mass complexes (filled circle) was observed below 500 nM She3p:Myo4p-C (2:1) subcomplex. (B and C) EMSAs with a constant concentration of ASH1-E3-77:She2p (2:4) subcomplex and increasing concentrations of She3p:Myo4p-C (2:1) subcomplex, similar to Fig. 2 B. The distinct band observed in lane 6 (double arrows and red boxes) indicates a saturated complex and suggests binding of two She3p:Myo4p-C complexes to one RNA-bound She2p tetramer. The experiment was performed with 125 nM (B) and 250 nM (C) ASH1-E3-77:She2p (2:4) subcomplex to rule out a concentration-dependent aggregation of the complex. Instead, these experiments confirm that the increase in size of the shifted bands (lanes 7 and 8, asterisks) is rather a result of excess She3p:Myo4p-C bound to the RNA in the SHE core complex. (D) Inversion of the experiment shown in B. Here, a constant concentration of the She3p:Myo4p-C (2:1) subcomplex was used, and increasing concentrations of the ASH1-E3-77:She2p (2:4) subcomplex were titrated. As before, the distinct band observed in lane 6 (double arrow and red box) indicates binding of two She3p:Myo4p subcomplexes to one RNA-bound She2p tetramer. Single arrows mark a substoichiometric SHE core complex. The asterisk marks a high molecular mass complex between the RNA in the SHE core complex and an excess of She3p:Myo4p-C with unspecific RNA-binding properties.

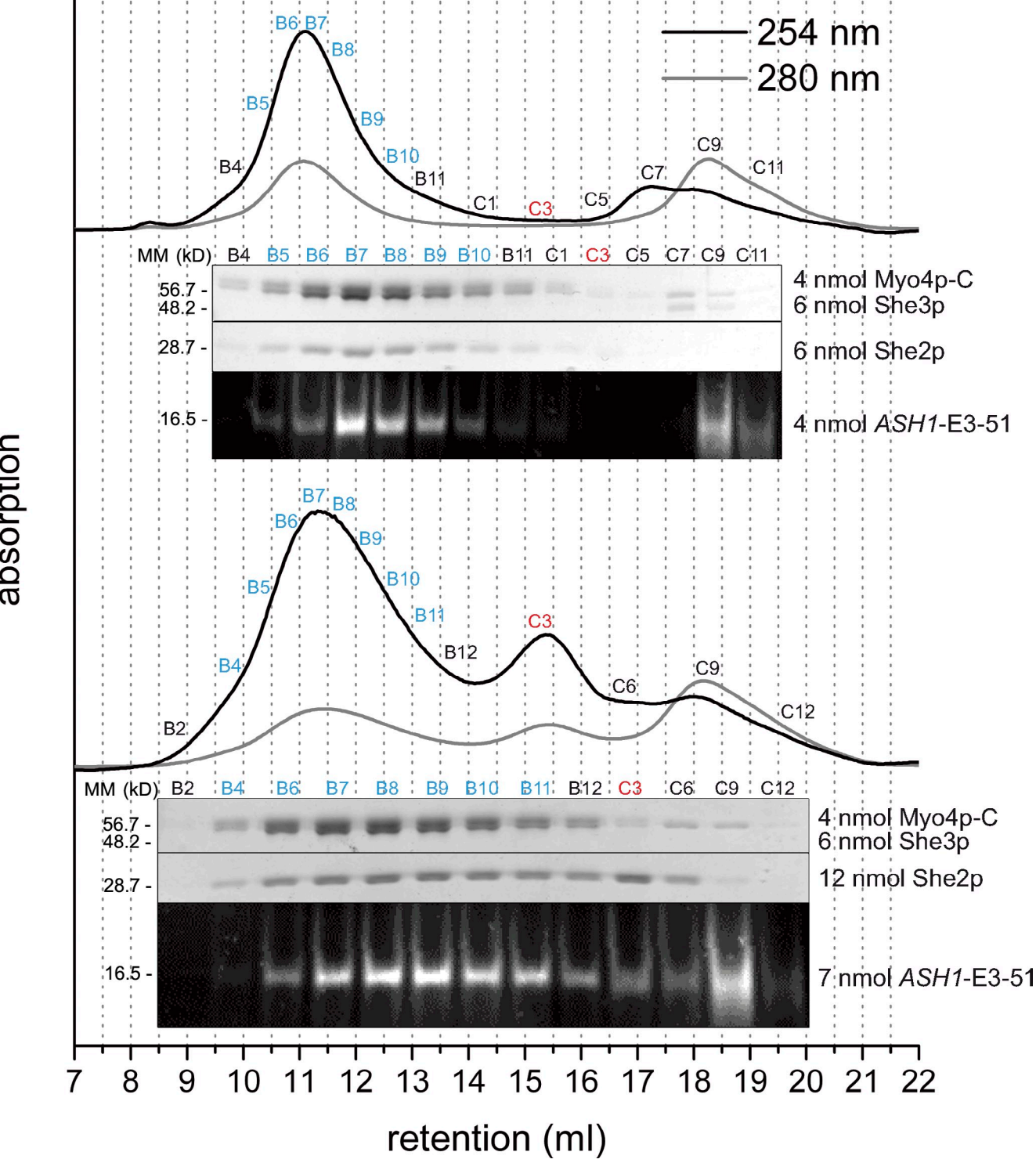


Figure S3. SEC to confirm the protein stoichiometries in the SHE core complex. (A) When equimolar amounts of She2p and She3p were used, a homogeneous SHE core complex (cyan) but no excess of ASH1-E3-51: She2p (red) was detected. (B) A twofold molar excess of She2p over She3p led to an excess of ASH1-E3-51:She2p (red) that was not in complex with She3p:Myo4p-C. These experiments indicate a 1:1 ratio between She2p and She3p in the SHE core complex. Amounts used for reconstitution are given on the right side. A slight excess of ASH1-E3-51 and Myo4p-C over She2p and She3p, respectively, was used to ensure complex saturation. Indicated fractions were analyzed by SDS-PAGE (proteins) with Coomassie blue staining and PAGE (RNA) with GelRed staining. Note that She3p and Myo4p-C migrate at a similar height in SDS-PAGE and appear as a double band. Black lines indicate that intervening lanes have been spliced out.

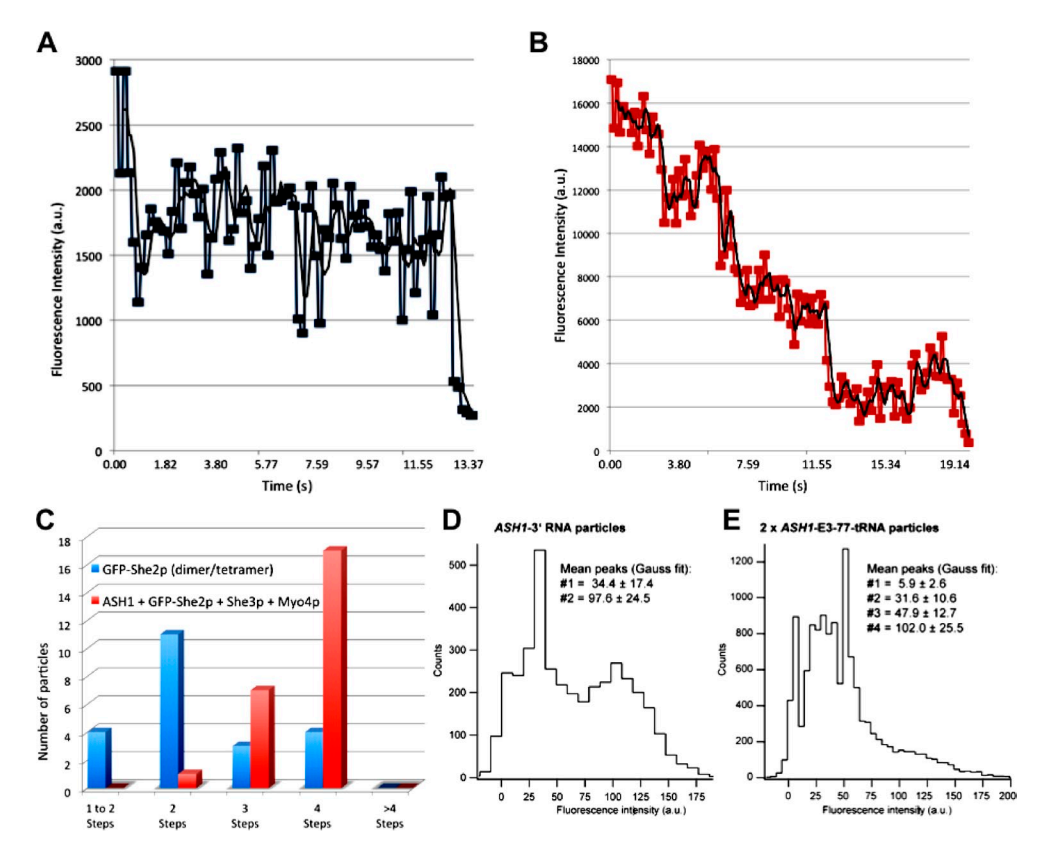


Figure S4. **Results from bleaching experiments.** (A and B) Photobleaching experiments with GFP-She2p only (A) and the reconstituted complex consisting of *ASH1-3'* + GFP-She2p + She3p + Myo4p (B). Shown are representative bleaching traces. The black line represents the mean of eight and seven consecutive bleaching points for A and B, respectively (C) Comparative plot of the number of bleaching steps per particle analyzed. As observed previously, at the given experimental conditions (i.e., 2 nM GFP-She2p), GFP-She2p exists in an equilibrium between dimeric and tetrameric states (Niessing et al., 2004; Müller et al., 2007). This, and the fact that some fluorophores are usually inactive, suggests that between one and four bleaching steps are to be expected. In the assembled motile complex (red), She2p becomes stabilized (Müller et al., 2011) and thus exists predominantly in the tetrameric form (this study; Krementsova et al., 2011). Because not a single particle (n = 30) shows more than four bleaching steps, we conclude that particles with a single zip code element indeed consist of a single SHE complex. (D and E) Histograms of fluorescence intensities from single-particle TIRFM experiments, showing the photobleaching behavior of motile SHE complexes containing *ASH1-3'* RNA (D) or the double zip code 2x *ASH1-E3-77-tRNA* RNA (E). From the Gaussian (Gauss) fit curves, the mean fluorescence intensity values for each population could be deduced. Although bleaching of *ASH1-3'* RNA particles (D) resulted from a single experiment each. For *ASH1-3'-77-tRNA* particles (E), twice as many populations (i.e., four) were identified. The shown data have been derived from a single experiment each. For *ASH1-3'-37-tRNA* particles (E), twice as many populations (i.e., four) were identified. The shown data have been derived from a single experiment each. For *ASH1-3'-37-tRNA* particles (E), twice as many populations (i.e., four) were identified. The shown data have been derived from a single experiment each. For *ASH1-3'-37-tRNA*

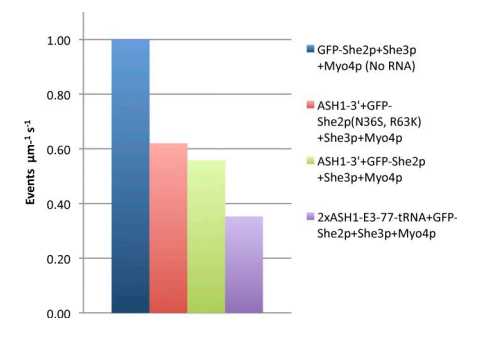
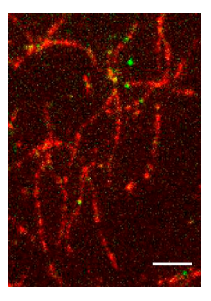
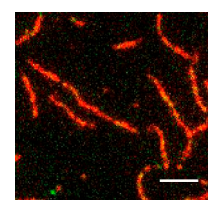


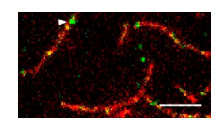
Figure S5. Comparison of motile events per micrometer actin and time from different SHE particles. Graph showing the run frequencies (n runs of the respective SHE complex per micrometer actin per second) in single-particle motility assays. Frequencies were normalized to frequencies of the SHE complex without RNA. The presence of RNA in the particles does not increase the number of processive SHE complexes on actin filaments. The presented data have been derived from a single experiment each and represent the same dataset analyzed in Fig. 4 F. For GFP-She2p + She3p + Myo4p (no RNA), n = 292; for ASH1-3' + GFP-She2p + She3p + Myo4p, n = 283; for ASH1-3' + GFP-She2p + She3p + Myo4p, n = 281; and for 2x ASH1-E3-77-IRNA + GFP-She2p + She3p + Myo4p, n = 320.



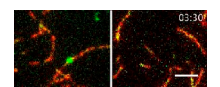
Video 1. Single-particle motility of a SHE complex consisting of ASH1-3' + GFP-She2p + She3p + Myo4p. GFP is shown in green, and TMR-labeled actin filaments are in red. TIRM images were taken with a TIRF microscope (IX50; Olympus) at room temperature at 4 frames/s and are displayed at 16 frames/s. The video was collected during the first 8 min of data acquisition. Arrowheads point out some of the observed processive runs. Bar, 5 µm. Video is related to Fig. 4 (A, E, and F).



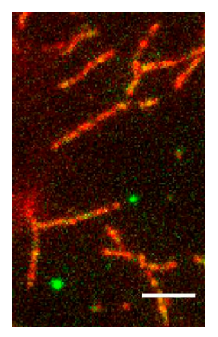
Video 2. **Single-particle motility of a SHE complex consisting of GFP-She2p + She3p + Myo4p.** GFP is shown in green, and TMR-labeled actin filaments are in red. TIRFM images were taken with a TIRF microscope (IX50; Olympus) at room temperature at 4 frames/s and are displayed at 16 frames/s. The video was collected during the first 8 min of data acquisition. Arrowheads point out processive runs. Bar, 5 µm. Video is related to Fig. 4 (B, E, and F).



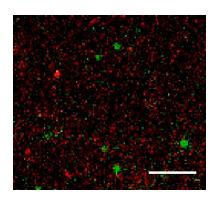
Video 3. Single-particle motility of a SHE complex consisting of the RNA binding-deficient GFP-She2p (N365, R63K) and She3p + Myo4p. GFP is shown in green, and TMR-labeled actin filaments are in red. TIRFM images were taken with a TIRF microscope (IX50; Olympus) at room temperature at 4 frames/s and are displayed at 16 frames/s. The video was collected during the first 8 min of data acquisition. Arrowheads point out processive runs. Bar, 5 µm. Video is related to Fig. 4 (C, E, and F).



Video 4. Single-particle motility of a SHE complex consisting of ASH1-3'+ GFP-She2p (ΔhE) + She3p + Myo4p. In this montage, SHE complexes containing the She3p-binding mutant GFP-She2p (ΔhE) (right) are compared with complexes containing wild-type GFP-She2p and no RNA (left). To ensure comparability between both experiments, image sequences start at the exact same time when each complex has been applied to the flow cell (i.e., 3 min). GFP is shown in green, and TMR-labeled actin filaments are in red. TIRFM images were taken with a TIRF microscope (IX50; Olympus) at room temperature at 4 frames/s and are displayed at 16 frames/s. As a result of size limitation, only every third frame is displayed. Bar, 5 μm. The time stamp indicates the total elapsed time since the beginning of the acquisition. The video was collected during the first 8 min of data acquisition. A full-size version of the video can be accessed via the JCB DataViewer. Video is related to Fig. 4 F. Time stamp indicates minutes and seconds.



Video 5. Single-particle motility of a SHE complex consisting of (2x E3-77-tRNA) + GFP-She2p + She3p + Myo4p. GFP is shown in green, and TMR-labeled actin filaments are in red. TIRFM images were taken with a TIRF microscope (IX50; Olympus) at room temperature at 4 frames/s and are displayed at 16 frames/s. The video was collected during the first 8 min of data acquisition. Arrowheads point out processive runs. Bar, 5 µm. Video is related to Fig. 4 (D–F).



Video 6. **Single-particle motility of a SHE complex consisting of Cy3.5-ASH1-E3-77 + Atto488-IST2 + She2p + She3p + Myo4p.** Cy3.5-labeled ASH1-E3-77 RNA is shown in red, and Atto488-labeled IST2 RNA is in green. Motility was assessed on unlabeled surface-attached F-actin. An example of individual ASH1-E3-77—and IST2-bound particles is pointed out by open red and green circles, respectively. Yellow open circles and arrowheads point to two processive runs where ASH1-E3-77 and IST2 are bound to the same SHE complex. TIRFM images were taken with a TIRF microscope (IX50; Olympus) at room temperature at 4 frames/s and are displayed at 16 frames/s. The video was collected during the first 8 min of data acquisition. Bar, 5 μm. Video is related to Fig. 4 F.

Table S1. List of She2p-dependently transported mRNAs

Yeast ID	Name	n/cell	Zip codes	Zip codes per cell (1 for unknown)	Zip codes per cell (2 for unknown)	Zip codes per cell (3 for unknown)	ORF + 100	MM (320/base)	Total MM
							bp	kD	kD
YKL185W	ASH1	88.00	4	352	352	352	1,867	597.4	52,574.7
YPL084W	BRO1	1.99	Unknown	1.99	3.98	5.97	2,635	843.2	1,678.0
YLR229C	CDC42	8.55	Unknown	8.55	1 <i>7</i> .1	25.65	676	216.3	1,849.5
YPR119W	CLB2	0.26	Unknown	0.26	0.52	0.78	1,576	504.3	131.1
YJL172W	CPS1	1.31	1	1.31	1.31	1.31	1,831	585.9	767.6
YLL001W	DNM1	2.08	2	4.16	4.16	4.16	2,374	759.7	1,580.1
YNL327W	EGT2	3.46	Unknown	3.46	6.92	10.38	3,226	1,032.3	3,571.8
YBR086C	IST2	2.05	1	2.05	2.05	2.05	2,941	941.1	1,929.3
YLR332W	MID2	3.23	Unknown	3.23	6.46	9.69	1,231	393.9	1,272.4
YLR190W	MMR1	0.19	Unknown	0.19	0.38	0.57	1,576	504.3	95.8
YFL005W	SEC4 (SRO6)	6.44	Unknown	6.44	12.88	19.32	748	239.4	1,541.5
YPR032W	SRO7	0.54	Unknown	0.54	1.08	1.62	3,202	1,024.6	553.3
YLL028W	TPO1	1.70	1	1.7	1.7	1.7	1,861	595.5	1,012.4
YNL283C	WSC2	4.00	2	8	8	8	1,612	515.8	2,063.4
YGR046W	TAM41	1.79	Unknown	1.79	3.58	5.37	1,258	402.6	720.6
YJL051C (YJL051W	IRC8	0.13	Unknown	0.13	0.26	0.29	2,569	822.1	106.9
YML072C	TCB3	3.11	Unknown	3.11	6.22	9.33	4,738	1,516.2	4,715.3
YMR171C	EAR1	1.47	Unknown	1.47	2.94	4.41	1,753	561.0	824.6
YNL087W	TCB2	2.11	Unknown	2.11	4.22	6.33	3,637	1,163.8	2,455.7
YGR040W	KSS1	1.28	Unknown	1.28	2.56	3.84	1,207	386.2	494.4
YMR296C	LCB1	6.56	Unknown	6.56	13.12	19.68	1,777	568.6	3,730.3
YNL103W	MET4	1.51	Unknown	1.51	3.02	4.53	2,119	678.1	1,023.9
Total		141.6		412	455	497			84,692

Localizing mRNAs were taken from Takizawa et al. (2000), Shepard et al. (2003), and Aronov et al. (2007). mRNAs that did not lose localization in SHE2 deletion strains or transcripts that have not been tested in this mutant were not considered. The numbers of transcripts per cell were taken from Miura et al. (2008), Nagalakshmi et al. (2008), and Pelechano et al. (2010), and the numbers for ASH1 mRNA were taken from Trcek et al. (2012). Numbers of zip code elements were taken from Chartrand et al. (1999), Gonzalez et al. (1999), Jambhekar et al. (2005), and Olivier et al. (2005). MM, molecular mass.

Table S2. Estimation of the number of SHE complexes per cell

Molecule	Copy number in complex	Copy number per cell	Complexes per cell	MM of components contributing to particles
She2p	4	4,070	1,017	
She3p	4	1,010	252	210,420 kD (proteins)
Муо4р	2	2,210	1,105	
Cmd1p/Mlc1p	12°	ND		
Zip code elements	2	450-500 ^b		
RNAs	Zip code dependent	142		84,692 kD ^b
Complex without RNA	835 kD	ND		All SHE complexes per cell \sim 300 mD

Copy numbers per cell were taken from Trcek et al. (2012). Bold numbers show the estimated molecular mass of all fully assembled SHE complexes in a cell. MM, molecular mass; ND, not determined.

bFor zip code and molecular mass calculation of mRNAs, see Table S1.

[°]Cmd1p/Mlc1p numbers are based on the assumption that each of the six IQ motifs of the Myo4p molecule is bound by one light chain.

Table S3. Plasmids used in this study

Plasmid name	Description	Source	PCR primers	Restriction sites
p01	pGEX-6p1 <i>SHE2</i>	Niessing et al., 2004		
p02	pET28a- <i>EGFP-SHE2</i>	This study	MMO16, MMO1	BamHI, XhoI
p10	pGEX-6P-1-SHE2-N36S- R63K	Du et al., 2008		BamHI, XhoI
RHP 27	pFastBacDual-SHE2/SHE3-His6	Müller et al., 2011		
AHP 2	pET28a- <i>SHE3(1-234)</i>	Heuck et al., 2007		
RHP 83	pGEX-6P-1- <i>SHE3(274–425)-His6</i>	This study	O49, O120	BamHI, EcoRI
AHP 7	pGEX-6P-1-MYO4(978-1471)	Heuck et al., 2007		
RHP 169	pFBDM-FLAG-MYO4-CMD1-MLC1- SHE3-HIS6-SHE4	This study	AHO149, AHO146; O209, O210 AHO94, AHO95, O239, O240, AH-O6,O118; O104, O105, O213, O214	, , ,
RHP 163	pET28a- <i>CMD1</i>	This study	O229, O230	Ncol, Xhol
RHP 167	pET28a-MLC1	This study	O237, O238	Ncol, Xhol
RHP 60	pBSMrna- <i>ASH1-E3-77</i>	Müller et al., 2011		Eagl, Sacll
RHP 149	pBSMrna- <i>IST2</i>	This study	0190, 0191	Eagl, Sacll
RHP 99	pBSMrna-HIV-1-TAR	This study	0134,0135	Eagl, Sacll
RHP 145	pBSMrna-2×- <i>ASH1-E3-77</i>	This study	0180, 0181, 0182, 0183	Eagl, Sacll
RHP 153	pBSMrna-ASH1-E3-77- HIV-1-TAR	This study	0180, 0198, 0199, 0200	Eagl, Sacll
RHP 166	pRS-405- <i>ASH1-3</i> ′	This study	ANO19, O233	Xhol, BamHl
FE#22	pET28a-EGFP-SHE2-N36S-R63K	This study; based on plasmid p02	P21, P22, P23, P24	BamHI, XhoI
FE#23	pET28a- <i>EGFP-SHE2-ΔhE</i> (deletion of amino acids 174–183)	This study; based on plasmid p02	P25, P26	BamHI, XhoI

pBSMrna (Ponchon et al., 2009); pFBDM (Berger et al., 2004).

Table S4. DNA oligonucleotides used in this study

Name	Primer sequence (5' $ ightarrow$ 3')
AHO6	AAAGGATCCATGTCGGACCAGGATAATACC
AHO94	AAACTCGAGATGTCCTCCAATCTTACCGAAGAA
AHO95	AAACCATGGCTATTTAGATAACAAAGCAGCGAA
AHO146	AAAGCGGCCGCTTATTTTCTGTCTAA
AHO149	AAAGGATCCATGGACTACAAGGACGATGACGAC
ANO19	AAAAAAGGATCCTGCGCAGGAGAAGTTATTAGAATGAT
MMO1	TTACTCGAGTCAGTTTTTCAATTTACCAAATTTG
MMO16	AAAGGATCCATGGGTACCTCAGCATGCAGTAAAGG
O49	TTTGAATTCCTAGTGATGGTGATGGGATTGGGCCCCCGTG
O104	GGTTCAGATACCAGTTCAAATTCAG
O105	CTGAATTTGAACTGGTATCTGAACC
O118	TTTTCTAGACTAATGATGGTGATG
O120	AAAGGATCCATGAGAAACGATGAGAAGATTAGTAATAAAG
O134	AAACGGCCGGGTCTCTCTGGTTAGACCAGATCTGAGCCTGGGAGCTCTCTGGCTAACTAGGGAACCTGGCCGCGGAAA
O135	TTTCCGCGGCCAGGTTCCCTAGTTAGCCAGAGAGCTCCCAGGCTCAGATCTGGTCTAACCAGAGAGACCCGGCCGTTT
O180	AAACGGCCGCCGTAACATAATTAGAGAATTGATACATGGATAACTGAATC
O181	GATTCAGTTATCCATGTATCAATTCTCTATATGTTAGAGAAATGTACAATTGTTTCGTG
O182	CACGAAACAATTGTACATTTCTCTAACATATAGAGAATTGATACATGGATAACTGAATC
O183	AAACCGCGGCCACCTTCTATAGAGAAATGTACAATTGTTTCGTG
O190	AAACGGCCGGATGCTGGAGTGAAGAATGTCACGAACAATTCTAAGACAACCGAATCCTCTTCCTCTTCATCTGGCCGCGGAAA
0191	TTTCCGCGGCCAGATGAAGAGGAAGAGGATTCGGTTGTCTTAGAATTGTTCGTGACATTCTTCACTCCAGCATCCGGCCGTTT
O198	CTGGTCTAACCAGAGAGACCATATGTTAGAGAAATGTACAATTGTTTCGTG
0199	CACGAAACAATTGTACATTTCTCTAACATATGGTCTCTCTGGTTAGACCAG
O200	TTTCCGCGGCCACCTTCTATGGTTCCCTAGTTAGCCAGAG
O204	TAATACGACTCACTATAGGGAGAGAATTGATACATGGATAACTG
O205	AGAGAAATGTACAATTGTTTCG
O209	CAGCGTTTCCCTGGGTCATCTGGATG
O210	CATCCAGATGACCCAGGGAAACGCTG
O213	AAACCCGGGATGCCACTGTGTGAG
0214	AAACCATGGTTAGACTTTAATTTTAGCAAGG
O229	AAACCATGGGCATGTCCTCCAATCTTACCG
O230	AAACTCGAGCTATTTAGATAACAAAGCAGCG
O233	CTCGAGCGAACTGCGAAATTG
O237	AAACCATGGGCATGTCAGCCACCAGAG
O238	AAACTCGAGTCATTGTCTCAAAACATCTTC
O239	AAAGGATCCATGTCAGCCACCAGAG
O240	AAATCTAGATCATTGTCTCAAAACATCTTC
P21	CATCTTATATTCACGTGCTGAGCAAGTTCATCAGTCATTTGCG
P22	CGCAAATGACTGATGAACTTGCTCAGCACGTGAATATAAGATG
P23	CTACTTTGATTAAATTTGTTAAGAAATTTGAAATTTTACAACGATTGTGTGTTAAGCTA
P24	TAGCTTAACACACAATCGTTGTAAAATTTCAATTTCTTAACAAATTTAATCAAAGTAG
P25	TCTCCGATATTCGTTCCGTCAACTTCTAAATCTAGCAGGTTGCTGC
P26	TGCTAGATTTAGAAGTTGACGGAACGAATATCGGAGAAACTG
P31	AATTTAATACGACTCACTATAGGGATGCTGGAGTGAAGAATGTC
P32	TTTTGGTTTTTCCTTTGCCGCCGATGAAGAGGAAGAGGATTC
P33	AATTTAATACGACTCACTATAGGGAGAGTTGATACATGGATAACTG
P34	GTAGTTTATTTAGCACAGGAGAGAAATGTACAATTGTTTCGTG
P37	AATTTAATACGACTCACTATAGGGCTACGTAGCTCAGTTG
P38	GTAGTTTATTTAGCACAGACAAGGTGGTGGCTACGACGGGATTC
P39	ATT0488-TTTTGGTTTTTCCTTTGCCGCC
P40	CY3.5-GTAGTTTATTTAGCACAGACAAGG

Bold labels indicate fluorophores attached to the respective primers.

Table S5. RNA sequences used in this study

RNA	Base rel. to start AUG	Sequence (5' $ ightarrow$ 3')	Produced by
ASH1-E3-51 (Müller et al., 2011)	1,771–1,821	AUGGAUAACUGAAUCUCUUUCAACUAAUAAGAGACAUUAUCACGAAAC AAU	Chemical synthesis (Thermo Fisher Scientific)
ASH1-E3-77	1,758–1,834	GGGAGAGAAUUGAUACAUGGAUAACUGAAUCUCUUUCAACUAAUAAGAGA CAUUAUCACGAAACAAUUGUACAUUUCUCU	In vitro transcription (template: produced by PCR with primers O204 and O205)
ASH1-E3-77-tRNA(Met) (Müller et al., 2011)	1,758–1,834	GGCUACGUAGCUCAGUUGGUUAGAGCAGCGGCCGAGAGAAUUGAUACAU GGAUAACUGAAUCUCUUUCAACUAAUAAGAGACAUUAUCACGAAACA AUUGUACAUUUCUCUUGGCCGCGGGUCACAGGUUCGAAUCCCGUCGU AGCCACCA	Expression in <i>E. coli</i>
ASH1-3' UTR*	1,695–1,998	GGGCGAAUUGGGUACCGGGCCCCCCUCGAGcgaacgcaacugcgaaau ugaaggGUACCGUUGCUUAUUUUGUAAUUACAUAACUGAGACAGUAGA GAAUUGAUACAUGAGACAGUAGA UAUCACGAAACAGUACAU UAUCACGAAACAAUUGUACAUUUCUCUCUUGUCUGUCUGCUAAAUAAA	In vitro transcription (template: RHP 166 linearized with BamHI and Nael)
IST2-tRNA	2,716–2,777	GGCUACGUAGCUCAGUUGGUUAGAGCAGCGGCCGGAUGCUGGAGUGAAGA AUGUCACGAACAAUUCUAAGACAACCGAAUCCUCUUCCUCUUCAUCUG GCCGCGGGUCACAGGUUCGAAUCCCGUCGUAGCCACCA	Expression in <i>E. coli</i>
HIV-1 TAR-tRNA		GGCUACGUAGCUCAGUUGGUUAGAGCAGCGGCCGGGUCUCUCUGGUUAGA CCAGAUCUGAGCCUGGGAGCUCUCUGGCUAACUAGGGAACCUGGCCGC GGGUCACAGGUUCGAAUCCCGUCGUAGCCACCA	Expression in <i>E. coli</i>
2×- <i>ASH1</i> -E3-77-fRNA	1,758–1,834	GGCUACGUAGCUCAGUUGGUUAGAGCAGCGGCCGCCGUAACAUAAUUAG AGAAUUGAUACAUGGAUAACUGAAUCUCUUUCAACUAAUAAGAGACA UUAUCACGAAACAAUUGUACAUUUCUCUAACAUAUAGAGAAUUGAUAC AUGGAUAACUGAAUCUCUUUCAACUAAUAAGAGACAUUAUCACGAAAC AAUUGUACAUUUCUCUAUAGAAGGUGGCCGCGGGUCACAGGUUCGAAU CCCGUCGUAGCCACCA	Expression in <i>E. coli</i>
<i>ASH1-</i> E3-77/HIV-1 TAR- tRNA	1,758–1,834	GGCUACGUAGCUCAGUUGGUUAGAGCAGCGGCCGCCGUAACAUAAUUAG AGAAUUGAUACAUGGAUAACUGAAUCUCUUUCAACUAAUAAGAGACA UUAUCACGAAACAAUUGUACAUUUCUCUAACAUAUGGUCUCUCUGGUU AGACCAGAUCUGAGCCUGGGAGCUCUCUGGCUAACUAGGGAACCAUAG AAGGUGGCCGCGGGUCACAGGUUCGAAUCCCGUCGUAGCCACCA	Expression in <i>E. coli</i>
IST2 + 22-nt 3' over- hang*	2,718–2,799	GGGAUGCUGGAGUGAAGAAUGUCACGAACAAUUCUAAGACAACCGAAUCC UCUUCCUCUUCAUCggcggcaaaggaaaaaccaaaa	In vitro transcription (template: produced by PCR with primers P31 and P32 on plasmid RHP 149)
ASH1-E3-77+ 24-nt 3' overhang*	1,758–1,858	GGGAGAGAAUUGAUACAUGGAUAACUGAAUCUCUUUCAACUAAUAAGAG ACAUUAUCACGAAACAAUUGUACAUUUCUCUccuugucugugcuaaa uaaacuac	In vitro transcription (template: produced by PCR with primers P33 and P34 on plasmid RHP 166)
2x-ASH1-E3-77-tRNA + 24-nt 3' overhang*	1,758–1,834	GGGCUACGUAGCUCAGUUGGUUAGAGCAGCGGCCGCCGUAACAUAAU <u>U</u> AGAGAAUUGAUACAUGGAUAACUGAAUCUCUUUCAACUAAUAAGA GACAUUAUCACGAAACAAUUGUACAUUUCUCU <u>AACAUAU</u> AGAGAAUUG AUACAUGGAUAACUGAAUCUCUUUCAACUAAUAAGAGACAUUAUCAC GAAACAAUUGUACAUUUCUCUAUAGAAGGUGGCCGCGGGUCACAGGUU CGAAUCCCGUCGUAGCCACCACCUUgucugugcuaaauaaacuac	In vitro transcription (template: produced by PCR with primers P37 and P38 on plasmid RHP 145)

Italic sequences mark nucleotides resulting from T7 transcription. Underlined sequences mark zip code or HIV-1 TAR sequences. Bold sequences mark three-way junction sequence from the Twort intron (Lescoute and Westhof, 2006). Small letters mark hybridization site for fluorescently labeled DNA-oligonucleotide binding. Asterisks mark RNAs used for single-particle motility assays in TIRFM.

References

- Aronov, S., R. Gelin-Licht, G. Zipor, L. Haim, E. Safran, and J.E. Gerst. 2007. mRNAs encoding polarity and exocytosis factors are cotransported with the cortical endoplasmic reticulum to the incipient bud in Saccharomyces cerevisiae. Mol. Cell. Biol. 27:3441–3455. http://dx.doi. org/10.1128/MCB.01643-06
- Berger, I., D.J. Fitzgerald, and T.J. Richmond. 2004. Baculovirus expression system for heterologous multiprotein complexes. *Nat. Biotechnol.* 22:1583–1587. http://dx.doi.org/10.1038/nbt1036
- Chartrand, P., X.H. Meng, R.H. Singer, and R.M. Long. 1999. Structural elements required for the localization of *ASH1* mRNA and of a green fluorescent protein reporter particle in vivo. *Curr. Biol.* 9:333–336. http://dx.doi.org/10.1016/S0960-9822(99)80144-4
- Du, T.G., S. Jellbauer, M. Müller, M. Schmid, D. Niessing, and R.P. Jansen. 2008. Nuclear transit of the RNA-binding protein She2 is required for translational control of localized ASH1 mRNA. EMBO Rep. 9:781–787. http://dx.doi.org/10.1038/embor.2008.112
- Gonzalez, I., S.B. Buonomo, K. Nasmyth, and U. von Ahsen. 1999. ASH1 mRNA localization in yeast involves multiple secondary structural elements and Ash1 protein translation. Curr. Biol. 9:337–340. http://dx.doi. org/10.1016/S0960-9822(99)80145-6
- Heuck, A., T.G. Du, S. Jellbauer, K. Richter, C. Kruse, S. Jaklin, M. Müller, J. Buchner, R.P. Jansen, and D. Niessing. 2007. Monomeric myosin V uses two binding regions for the assembly of stable translocation complexes. *Proc. Natl. Acad. Sci. USA*. 104:19778–19783. http://dx.doi.org/10.1073/pnas.0706780104
- Jambhekar, A., K. McDermott, K. Sorber, K.A. Shepard, R.D. Vale, P.A. Takizawa, and J.L. DeRisi. 2005. Unbiased selection of localization elements reveals cis-acting determinants of mRNA bud localization in *Saccharomyces* cerevisiae. Proc. Natl. Acad. Sci. USA. 102:18005–18010. http://dx.doi. org/10.1073/pnas.0509229102
- Krementsova, E.B., A.R. Hodges, C.S. Bookwalter, T.E. Sladewski, M. Travaglia, H.L. Sweeney, and K.M. Trybus. 2011. Two single-headed myosin V motors bound to a tetrameric adapter protein form a processive complex. J. Cell Biol. 195:631–641. http://dx.doi.org/10.1083/jcb.201106146
- Lescoute, A., and E. Westhof. 2006. Topology of three-way junctions in folded RNAs. RNA. 12:83–93. http://dx.doi.org/10.1261/rna.2208106
- Miura, F., N. Kawaguchi, M. Yoshida, C. Uematsu, K. Kito, Y. Sakaki, and T. Ito. 2008. Absolute quantification of the budding yeast transcriptome by means of competitive PCR between genomic and complementary DNAs. BMC Genomics. 9:574. http://dx.doi.org/10.1186/1471-2164-9-574
- Müller, M., A. Heuck, and D. Niessing. 2007. Directional mRNA transport in eukaryotes: lessons from yeast. Cell. Mol. Life Sci. 64:171–180. http:// dx.doi.org/10.1007/s00018-006-6286-1
- Müller, M., R.G. Heym, A. Mayer, K. Kramer, M. Schmid, P. Cramer, H. Urlaub, R.P. Jansen, and D. Niessing. 2011. A cytoplasmic complex mediates specific mRNA recognition and localization in yeast. *PLoS Biol.* 9:e1000611. http://dx.doi.org/10.1371/journal.pbio.1000611
- Nagalakshmi, U., Z. Wang, K. Waern, C. Shou, D. Raha, M. Gerstein, and M. Snyder. 2008. The transcriptional landscape of the yeast genome defined by RNA sequencing. *Science*. 320:1344–1349. http://dx.doi.org/10.1126/science.1158441
- Niessing, D., S. Hüttelmaier, D. Zenklusen, R.H. Singer, and S.K. Burley. 2004. She2p is a novel RNA binding protein with a basic helical hairpin motif. Cell. 119:491–502. http://dx.doi.org/10.1016/j.cell.2004.10.018
- Olivier, C., G. Poirier, P. Gendron, A. Boisgontier, F. Major, and P. Chartrand. 2005. Identification of a conserved RNA motif essential for She2p recognition and mRNA localization to the yeast bud. *Mol. Cell. Biol.* 25:4752–4766. http://dx.doi.org/10.1128/MCB.25.11.4752-4766.2005
- Pelechano, V., S. Chávez, and J.E. Pérez-Ortín. 2010. A complete set of nascent transcription rates for yeast genes. PLoS ONE. 5:e15442. http://dx.doi. org/10.1371/journal.pone.0015442
- Ponchon, L., G. Beauvais, S. Nonin-Lecomte, and F. Dardel. 2009. A generic protocol for the expression and purification of recombinant RNA in *Escherichia coli* using a tRNA scaffold. *Nat. Protoc.* 4:947–959. http:// dx.doi.org/10.1038/nprot.2009.67
- Shepard, K.A., A.P. Gerber, A. Jambhekar, P.A. Takizawa, P.O. Brown, D. Herschlag, J.L. DeRisi, and R.D. Vale. 2003. Widespread cytoplasmic mRNA transport in yeast: identification of 22 bud-localized transcripts using DNA microarray analysis. *Proc. Natl. Acad. Sci. USA*. 100:11429–11434. http://dx.doi.org/10.1073/pnas.2033246100

- Takizawa, P.A., J.L. DeRisi, J.E. Wilhelm, and R.D. Vale. 2000. Plasma membrane compartmentalization in yeast by messenger RNA transport and a septin diffusion barrier. *Science*. 290:341–344. http://dx.doi.org/10.1126/science.290.5490.341
- Trcek, T., J.A. Chao, D.R. Larson, H.Y. Park, D. Zenklusen, S.M. Shenoy, and R.H. Singer. 2012. Single-mRNA counting using fluorescent in situ hybridization in budding yeast. *Nat. Protoc.* 7:408–419. http://dx.doi. org/10.1038/nprot.2011.451